Forensic Science International: Genetics 78 (2025) 103274

Contents lists available at ScienceDirect

Forensic Science International: Genetics

journal homepage: www.elsevier.com/locate/fsigen

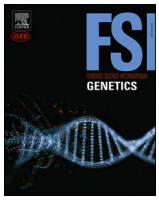

Mitochondrial genome sequencing with ForenSeq™ mtDNA Whole Genome Kit

Jinfeng Xuan [a], Guannan Long [b], Haiduo Wu [b], Ze Liu [b], Biao Zhang [b], Shaobo Yu [b,**], Fu Ren [c,d,e,*], Fei Guo [c,d,e,*]

[a] School of Forensic Medicine, China Medical University, Shenyang, Liaoning 110122, PR China
[b] DNA Laboratory of Forensic Science Center, Shenyang Public Security Bureau, Shenyang, Liaoning 110002, PR China
[c] Shenyang Medical College, Shenyang, Liaoning 110034, PR China
[d] Liaoning Province Key Laboratory for Phenomics of Human Ethnic Specificity and Critical Illness (LPKL-PHESCI), Shenyang, Liaoning 110034, PR China
[e] Shenyang Key Laboratory for Phenomics, Shenyang, Liaoning 110034, PR China

ARTICLE INFO

Keywords:
Massively parallel sequencing (MPS)
Mitochondrial genome (mtGenome)
ForenSeq™ mtDNA Whole Genome Kit
MiSeq FGx® Sequencing System
Internal validation

ABSTRACT

Mitochondrial DNA (mtDNA) possesses unique genetic characteristics and plays a crucial role in forensic DNA analysis. Based on the massively parallel sequencing (MPS) technology alongside the short overlapping amplicon method, the ForenSeq™ mtDNA Whole Genome Kit is specifically designed for mtDNA analysis. In this study, we employ the ForenSeq™ mtDNA Whole Genome Kit on the MiSeq FGx® Sequencing System for mitochondrial genome (mtGenome) sequencing across nine consecutive runs and assess its MPS performance, such as read depth (RD), forward/reverse strand bias (SB), and mtGenome coverage. Furthermore, we conduct internal validations to evaluate its routine application in forensic sciences, including sensitivity, repeatability, concordance, degraded samples, inhibitor samples, case-type samples, and contamination. As a result, the Real-Time Analysis (RTA) and Universal Analysis Software (UAS) demonstrate proficient run metrics and MPS performance when 12–14 libraries are sequenced within a standard flow cell, achieving > 80 % of reads passing filter, > 80 % bases with ≥Q30, > 5000 × of the average RD, ~1.0 of the average SB, > 70 % of the inter-amplicon balance, and > 99 % of the mtGenome coverage. The five most vulnerable amplicons, exhibiting low RD and high SB, are identified as nucleotide positions (nps) 1094–1177, 5858–5975, 6109–6149, 6718–6810, and 7021–7090. For tertiary data analysis, the substitutions are accurately reported by UAS, while insertions and deletions (indels), point heteroplasmies (PHPs), and/or length heteroplasmies (LHPs) still necessitate manual inspection. On average, 40 variants were found in 60 samples, ranging from 27 to 54. A total of 2426 variants are observed at 491 nps. Moreover, the workflow can yield repeatable and reproducible results, generate complete mtGenome profiles from ≥ 2 pg input gDNA for high quality samples/control DNA or ≥ 0.5 cm hair shafts, and recover more/complete mtGenome information from severely degraded samples (degradation index >10) and various types of case samples. If two rounds of purification are conducted, it can more effectively remove additional reaction components and enhance data recovery from the mtGenome, especially for low-input samples. The negative controls in three runs cover some reads, but these contaminations cannot compromise the mitochondrial analyses. In conclusion, the ForenSeq™ mtDNA Whole Genome Kit, including 234 short overlapping amplicons with an average size of 131 bp, can meet forensic needs on the whole mtGenome sequencing in real scenarios. In addition, the ten insights gained from this study may serve as a valuable reference for forensic scientists who are utilizing this kit.

1. Introduction

Unlike nuclear DNA (nDNA), human mitochondrial DNA (mtDNA) is a circular double-stranded molecule in mitochondria. It has a total length of about 16569 base pairs (bp) and is divided into two chains - the heavy chain (H chain) and the light chain (L chain). The non-coding

* Corresponding authors at: Shenyang Medical College, Shenyang, Liaoning 110034, PR China.
** Correspondence to: Shenyang Public Security Bureau, Shenyang, Liaoning 110002, PR China.
E-mail addresses: 243816450@qq.com (S. Yu), rf@symc.edu.cn (F. Ren), nevergfaye@gmail.com (F. Guo).

https://doi.org/10.1016/j.fsigen.2025.103274
Received 19 December 2024; Received in revised form 18 February 2025; Accepted 13 March 2025
Available online 17 March 2025

control region (CR), also known as the D-loop, is 1122 bp long and contains three hypervariable segments (HVS) that exhibit high polymorphisms [1]. The coding region (CodR) is 15447 bp long and encodes 22 transfer RNA (tRNA) genes, 2 ribosomal RNA (rRNA) genes, and 13 protein genes, in which pathogenic mutations are closely related to various diseases in clinical research [2]. In addition to being inherited from the maternal line as the haplotype, mtDNA possesses several unique genetic characteristics, such as high copy number (~1000 copies per cell), high mutation rate (~5–10 times higher than nDNA), and excellent structural stability, which make it an important role in forensic DNA analysis [1].

With the advancement of massively parallel sequencing (MPS) technology, the focus of forensic mtDNA analysis has shifted from HVS or CR with capillary electrophoresis (CE)-based Sanger sequencing [3] to mitochondrial whole genome (mtGenome) [4–14,17–33]. Over the past decade, new sequencing strategies and platforms have been introduced, greatly accelerating the forensic application of mtGenome. In forensics, the polymerase chain reaction (PCR)-based method is a commonly used strategy for enriching mtGenome libraries, including long and short amplicon methods. The long amplicon method typically involves about two 8 kbp or eight 1–3.5 kbp overlapping amplicons for shotgun sequencing on the Ion Torrent PGM™ [4–6], Illumina MiSeq® [7–12], Roche 454 GS Junior [13], and MGISEQ-200RS platforms [14], which is well-suited for specimens with DNA sufficient in quality and quantity. On the other hand, the short amplicon method typically involves dozens to hundreds of 100–500 bp overlapping amplicons divided into two multiplexes for targeted sequencing [12], which is more suitable for degraded samples or trace samples. In archaeology, non-PCR-based strategies such as primer extension capture (PEC) [15] or hybridization capture [16] are also used for sequencing to retrieve ancient DNA (aDNA) that are heavily degraded and contaminated specimens with microbial DNA, as is typical of ancient bones [17,18]. The forensic manufacturers released commercial kits based on the short amplicon method, such as the Precision ID mtDNA Whole Genome Panel on the Ion GeneStudio S5™ Plus System by Thermo Fisher Scientific [19–30] and ForenSeq™ mtDNA Whole Genome Kit on the MiSeq FGx® Sequencing System by Qiagen [31–33]. Further, recent advancements in the accuracy of long-read sequencing technologies (e.g., Oxford Nanopore Technologies and Pacific Biosciences Sequel II) have prompted the use of mtGenome sequencing [34,35].

The ForenSeq™ mtDNA Whole Genome Kit consists of two primer sets, each with 117 primer pairs, generating 234 short overlapping amplicons with an average size of 131 bp (90–209 bp including primers) and an average amplicon overlap of 14 bp (0–71 bp). Additionally, each primer set contains degenerate primers, 111 in Whole Genome Mix Set 1 (WGS1) and 97 in Whole Genome Mix Set 2 (WGS2), to account for known variants (with >1 % frequencies reported in MITOMAP) located in primer-binding regions in order to reduce the risk of amplicon dropout. In 2021, the design and developmental validation of this kit were first reported by Holt *et al.* [31] on aspects of species specificity, sensitivity, stability, reproducibility and repeatability, case-type samples, population, mixture, PCR-based, and MPS-specific studies. The same year, Peng *et al.* [32] evaluated this kit's performance and applied it to detect the mtGenome in blood samples and hair shafts from 2–4 generation maternal pedigrees. In 2023, Liu *et al.* [33] assessed this kit in sensitivity and case-type samples for forensic application. In this study, we employed the ForenSeq™ mtDNA Whole Genome Kit on the MiSeq FGx® Sequencing System for mtGenome sequencing across 9 consecutive runs and assessed its MPS performance (i.e., read depth, strand bias, and mtGenome coverage both at nucleotide positions and amplicons). Additionally, we performed internal validations (except for mixture studies) to evaluate its routine application in forensic sciences, including sensitivity, repeatability, concordance, degraded samples, inhibitor samples, case-type samples, and contamination according to 'Validation Guidelines for DNA Analysis Methods (2016)' issued by the Scientific Working Group on DNA Analysis Methods (SWGDAM) [36].

2. Materials and methods

2.1. Sample preparation

2.1.1. Sensitivity studies

Serial dilutions of 100 pg, 50 pg, 20 pg, 10 pg, 5 pg, and 2 pg were prepared with the Control DNA HL60 (Qiagen, Hilden, Germany). One set of serial dilutions was purified using one round of purification, and the other set was purified with two rounds of purification. These two sets were sequenced on two separate flow cells along with other samples.

2.1.2. Repeatability and concordance studies

Four purified samples were used in this study: the Control DNA 007 (Thermo Fisher Scientific, MA, USA), 2800M Control DNA (Promega, WI, USA), Control DNA 9947A (Thermo Fisher Scientific), and 9948 Male DNA (Promega). Two sets of libraries were prepared for the samples and sequenced on two separate flow cells. The Control DNA HL60 was also employed as a positive control (PTC) in each run to evaluate repeatability and concordance.

2.1.3. Degraded samples

Muscle tissue was cut into small pieces of uniform size and then soaked in tap water in a 15 mL centrifuge tube. This tube was then tightly capped and placed indoors at room temperature for 3, 6, and 9 days. At each time point, one piece of tissue was removed and immediately subjected to DNA extraction on the AutoMate Express™ Forensic DNA Extraction System (Thermo Fisher Scientific) with an elution volume of 100 μL for each piece. Untreated muscle DNA was employed as a PTC.

2.1.4. Inhibitor samples

Inhibitor samples were mocked using swab samples containing 100 μM hematin and extracted using an Ultra Micro Magnetic Bead DNA Extraction Kit on an Automatic 96 Channel Micro DNA Extraction Workstation (Bokun Biotech, Changchun, China).

2.1.5. Nail, tooth, and bone samples

Nail, tooth, and bone samples were collected from routine casework. The clipped nail (~8 mm × 2 mm cut into two pieces) and powdered tooth (~50 mg) and bone (~50 mg) were digested with 190 μL PrepFiler BTA™ Lysis Buffer (Thermo Fisher Scientific), 10 μL Proteinase K (PK; Thermo Fisher Scientific), and 7 μL of 10 mM dithiothreitol (DTT; Inalco, Milano, Italy) in 1.5 mL Eppendorf tubes and then incubated in a thermomixer (Eppendorf, Hamburg, Germany) at 56 °C and 800 rpm for 4 h (nail) and 12 h (tooth and bone). Subsequently, 10 μL PK and 7 μL DTT were again added to the tooth and bone samples, and digestion was continued for at least an additional 12 h. Finally, all samples were incubated at 99 °C and 800 rpm for 10 min and transferred to DNA purification on the AutoMate with an elution volume of 40 μL.

2.1.6. Hair shaft and buccal swab samples

Nine head hairs in total were collected from two laboratory staff: four undyed hairs representing one individual (sample G) and one gray and four undyed hairs representing the other individual (sample L). Approximately 2 cm of each hair's root end was removed, while the remaining proximal hair shafts (next to the root) were cut into 2 cm, 1 cm, and 0.5 cm segments, and the distal hair shafts (next to the tip) were cut into 2 cm. Each segment was sequentially rinsed with 1 % sodium dodecyl sulfate (SDS; Solarbio, Beijing, China), 6 % sodium hypochlorite (NaClO; Xilong Scientific, Guangdong, China), RT-PCR grade water (Thermo Fisher Scientific), and 100 % ethyl alcohol (Sigma-Aldrich, MO, USA) using sterile forceps. Hair samples were digested with 190 μL PrepFiler BTA™ Lysis Buffer, 10 μL PK, and 7 μL DTT and then incubated in a thermomixer at 56 °C and 800 rpm for at least 4 h until they were completely dissolved. At last, all tubes were incubated at 99 °C and 800 rpm for 10 min and transferred to DNA

purification on the AutoMate with an elution volume of 30 μL. At the same time, buccal swab samples were collected as PTCs.

2.1.7. MPS performance

MPS performance in five batch tests was evaluated using peripheral blood samples of 60 unrelated healthy individuals collected from Liaoning Province. All information regarding the nature of the research study for which their samples were used was shared with participants, and then all participants signed the informed consent form and agreed to the results published in scientific publications. This study was approved by the Medical Ethics Committee of China Medical University (No. [2023] 043).

2.2. DNA extraction and quantification

All samples were extracted and purified using the PrepFiler Express BTA™ Forensic DNA Extraction Kit (Thermo Fisher Scientific) on the AutoMate Express™ Forensic DNA Extraction System according to the manufacturer's recommendations [37]. Genomic DNA (gDNA) and degradation index (DI) were quantified and measured on the Applied Biosystems® QuantStudio 5 Real-time PCR System (Thermo Fisher Scientific) using the Quantifiler® Trio DNA Quantification Kit according to the user guide [38]. All extracted and quantified DNA was stored at –20 °C.

2.3. Library preparation

Library preparation was performed using the ForenSeq™ mtDNA Whole Genome Kit (Qiagen) according to the manufacturer's recommendations [39], mainly including six steps as follows:

(1) Amplify and tag targets: 12 μL of each diluted gDNA (8.33 pg/μL) were split across two amplifications (50 pg each for a total of 100 pg); otherwise, 12 μL extracts were directly used, e.g., sensitivity dilutions (50–2 pg total), nail (36 pg total), tooth (72 pg total), and hair samples (gDNA not quantifiable). Amplification was performed in a volume of 15 μL containing 3.7 μL mtPCR1 Reaction Mix, 0.3 μL ForenSeq Enzyme Mix (FEM), and 5 μL WGS1 or WGS2 on the ProFlex™ PCR System (Thermo Fisher Scientific) using the thermal cycling conditions of enzyme activation for 3 min at 98 °C, amplification for 8 cycles of 45 s at 96 °C, 10 s at 80 °C, 2 min at 54 °C (ramp mode of 0.2 °C/s), 1.5 min at 66 °C (ramp mode of 0.2 °C/s) and 10 cycles of 30 s at 96 °C, 2 min at 68 °C (ramp mode of 0.2 °C/s), extension for 10 min at 68 °C, and hold at 10 °C forever.

(2) Enrich targets: A total of 4 μL Index 1 (i7) adapters, 4 μL Index 2 (i5) adapters, and 27 μL mtPCR2 Reaction Mix were consecutively added into each amplified target and then incubated for 30 s at 98 °C, 15 cycles of 20 s at 98 °C, 30 s at 66 °C and 1.5 min at 68 °C, 10 min at 68 °C, and hold at 10 °C forever.

(3) Purify libraries: Enriched libraries from WGS1 and WGS2 were pooled together and then purified using 90 μL Sample Purification Beads 2/Proteinase K (SPB2/ProK) and 80 % fresh ethanol (EtOH) and then added 52.5 μL Resuspension Buffer (RSB). Herein, libraries from one set of sensitivity dilutions, repeatability, concordance, degraded samples, inhibitor samples, and case-type samples were performed with the optional second purification; otherwise, libraries were purified once. Some purified libraries were quantified with the Qubit™ dsDNA HS Assay Kit on the Qubit™ 4.0 Fluorometer (Thermo Fisher Scientific) according to the manufacturer's recommendations [40].

(4) Normalize libraries using a bead-based method: Each 20 μL purified library was mixed with a 45 μL master mix of Library Normalization Additives 1 (LNA1) and Library Normalization Beads 1 (LNB1), then washed twice using 45 μL Library Normalization Wash 1 (LNW1), and mixed with 32 μL 0.1 N NaOH (HP3). Finally, each 30 μL Library Normalization Storage Buffer 2 (LNS2) was added to the 30 μL normalization library.

(5) Pool libraries: Normalized libraries were pooled in equal volumes (5 μL), but the number of pooled libraries depends on the data quality required. Although the manufacturer's protocol recommended that the maximum number of 16 libraries can be supported with the MiSeq FGx standard flow cell, 10–12 libraries along with one PTC and one negative control (NTC) were pooled in this study.

(6) Denature and dilute libraries (this step was modified): 5 μL pooled libraries was added into 600 μL Hybridization Buffer (HT1) and then mixed with 4 μL HP3-denatured Human Sequencing Control (HSC). The diluted normalized libraries (DNL) tube was placed on a thermomixer at 96 °C for 2 min and immediately in the ice-water bath for 5 min. There are two reasons for the modification. The first is that the actual volume is less than 5 μL when transferring pooled libraries from the pooled normalized libraries (PNL) tube on the preheated heat block into the DNL tube, possibly due to the thermal expansion and contraction effect. The second is that HSC did not meet the criteria of over intensity and discordant loci in the demo test, which may be associated with inadequate (only HP3 but no heat) denaturation.

2.4. Cluster generation, sequencing, and data analysis

Cluster generation and sequencing were performed using the Forensic Genomics run mode on the MiSeq FGx® Sequencing System (Qiagen) and the MiSeq FGx® Reagent Kit following the manufacturer's instruction [41]. The entire volume of denatured libraries was loaded onto the reagent cartridge and sequenced with 2 × (201 + 8) cycles.

During sequencing, the Real-Time Analysis (RTA) performed primary data analysis for calling bases and assigning quality scores. RTA quality metrics were viewed by the Sequencing Analysis Viewer Software (SAV) v1.9.1 (Illumina, CA, USA). After a run was complete, secondary data analysis was automatically processed using the Verogen mtDNA Whole Genome Analysis Method in the Universal Analysis Software (UAS) v2.5.1 (Qiagen) [42] with some modifications: 6 % of Analytical Threshold, 10 % of Interpretation Threshold, 30 of Minimum Quality Score, and 45 of Minimum Read Count. This process involves demultiplexing the samples based on the index combinations, generating FASTQ files from the demultiplexed binary base call (BCL) files for each sample, aligning raw reads to the revised Cambridge Reference Sequence (rCRS, NC_012920.1) using the maximal exact matches algorithm of the Burrows-Wheeler Aligner (BWA-MEM), removing known nuclear mitochondrial DNA segments (NUMTs) in the reference human NumtS (RHNumtS) compilation and the human mitochondrial database (HmtDB), screening mixed base positions using the Basic Local Alignment Search Tool (BLAST) analysis, trimming low-quality nucleotides, < 40-nucleotide amplicons, primers, and/or adapter dimers, and calling variants using forensic rules and SWGDAM nomenclature [31]. Tertiary data analysis was conducted using the Integrative Genomic Viewer (IGV) package v.2.16.0 [43] if there were no calls, transversions, insertions and deletions (indels), point heteroplasmies (PHPs), and/or length heteroplasmies (LHPs). Herein, binary alignment map (BAM) and binary alignment index (BAI) files were stored in the *D:\verogen\fuas\runs\run number\analyses\sample number\analyses number* folder. The 3107DEL called by UAS was revised to N3107 in all samples.

The rCRS-format reports were generated in the UAS for samples after manual inspection. The preliminary haplogroup assignment was enrolled from the highest-ranked haplogroup from HaploGrep 3 [44] and EMMA [45] in the European DNA Profiling Group Mitochondrial DNA Population Database (EMPOP) v4/R13, respectively. Missing mutations and extra mutations were double-checked using IGV. The final haplogroup assignment was determined according to the rCRS-oriented version of the mtDNA PhyloTree Build 17 [46] and the EMPOP QC

Report [47].

2.5. Statistics

The read depth (RD) was defined by summing all reads at a mitochondrial nucleotide position (np). The amplicon RD balance was calculated by comparing the RD of an amplicon (without upstream and downstream overlaps) to the average RD of all amplicons (without upstream and downstream overlaps), with 1.0 indicating an amplicon with a balanced RD [27]. The inter-amplicon balance was assessed as the proportion of amplicons with the value of the amplicon RD balance > 0.20. The strand bias (SB) was calculated as the ratio of forward to reverse strand reads (#F/#R) at a particular np. The amplicon SB balance (without upstream and downstream overlaps) was measured as 1 − (the strand direction with the smaller number of reads/the strand direction with the larger number of reads), i.e., 1 − (#S/#L), with 0 indicating no SB of an amplicon and 1.0 indicating the presence of reads in only one direction [27]. The percentage of mtGenome coverage for a sample was estimated by dividing the total number of detectable nps by the expected 16569 nps. All values were extracted from a VCF file in the *D:\verogen\fuas\runs\run number\analyses\sample number\analyses number* folder generated by UAS. One-way analysis of variance (ANOVA), F-statistic test, Wilcoxon rank test, and proportion test were performed using R version 4.3.1 [48]. Circos plots were generated by TBtools-II v2.070 [49], and other charts were done by Excel 2021 (Microsoft, WA, USA).

3. Results and discussion

3.1. Run-level performance

The RTA quality metrics extracted from SAV are listed in Table S1,

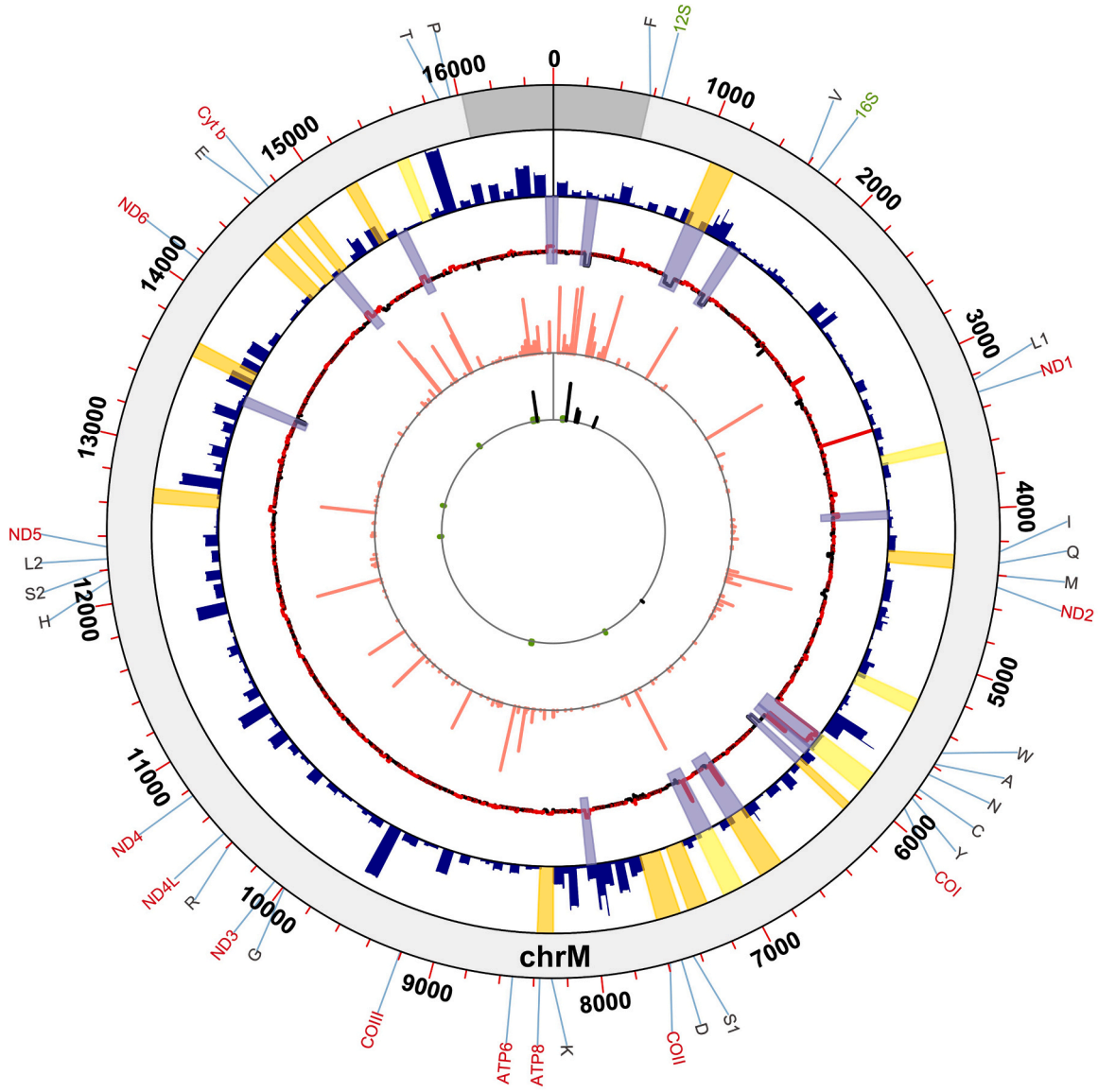

Fig. 1. MPS performance and variant distribution. A Circos plot of the mitochondrial genome (mtGenome) representing the coding genes (the first circle; n = 37; transfer RNA, ribosomal RNA, and protein genes abbreviated in black, green, and red, respectively), the nucleotide positions (the second circle; n = 16569; the control region and the coding region masked in dark grey and light grey, respectively), the average read depth (RD; the third circle; n = 60; the extremely low amplicon RD masked in orange and the relatively low amplicon RD masked in yellow), the forward/reverse strand balance (SB; the fourth circle; n = 60; SB > 1.0 indicated in red and SB < 1.0 indicated in black; the low-performing amplicon masked in purple), and the variant distribution (the fifth circle; n = 2426), and the point heteroplasmy (PHP; n = 12; green) and length heteroplasmy (LHP; n = 36; black) distribution (the sixth circle). Details of amplicon RD and SB, genes and variants, PHPs, and LHPs are listed in Table S2, Table S3, Table S5, and Table S6, respectively.

including the number of bases sequenced (i.e., yield total), the number of clusters (i.e., reads), the number of clusters passing filtering (i.e., reads PF), and the percentage of bases with a quality score of 20 or 30 or higher (i.e., %≥Q20 and %≥Q30, respectively) across 418 cycles on 19 tiles, and the mean ± standard deviation (SD) across the 9 runs were calculated as 5.2 G ± 0.9 G, 14.06 M ± 2.93 M, 12.60 M ± 2.60 M, 89.36 % ± 3.60 %, and 82.27 % ± 4.85 %, respectively. The UAS quality metrics in each run fell within the recommended range with some exceptions, including PTCs (16570 positions called and ≥400 K passing filter reads for HL60), NTCs (0 positions called except for Run 4&7), run quality metrics (400–1650 K/mm^2 of cluster density, ≥80 % of clusters passing filter, ≤0.25 % of phasing except for Run 3, and ≤0.15 % of prephasing), read and index quality metrics (read 1, index 1, index 2, and read 2), and human sequencing control (over intensity and 0 discordant loci). The run quality metrics presented on UAS are also summarized in Table S1, where the mean ± SD across the 9 runs were 1180 K/mm^2 ± 263 K/mm^2, 90.27 % ± 3.65 %, 0.217 % ± 0.029 %, and 0.094 % ± 0.027 %, respectively. Herein, the phasing (0.279 %) in Run 3 is labeled as out of the recommended range and may be associated with inhibitors existed (discussed in Section 3.4.4). Two variants called for NTCs in Run 4&7 will be explained in Section 3.4.6. Overall, the RTA and UAS quality metrics assessment revealed high-quality runs with excellent performance.

3.2. Sample-level performance

As shown in Figure S1, 86.67 % (52/60) of samples in five batch tests (Run 5–9) passed the sample read count guideline (400000 ×). The average sample intensity presented on UAS was 537671 × ± 118040 ×, which was similar to the results of the same kit reported by Peng *et al.* [32]. Fig. 1 displays that the sample-level performance was evaluated on the average RD and average SB at each mitochondrial np from 60 samples. Table S2 and Figure S2 show the average RD and SB of 234 numbered amplicons (without upstream and downstream overlaps). The average RD and average SB of the control and coding regions are summarized in Table S3.

3.2.1. Read depth

In regards to the RD, the mean ± SD was calculated to 5084 × ± 6904 × across 16569 nps, which was higher than those using the long amplicon method [5–8,13]. Herein, 100 % (16569/16569) and 98.24 % (16277/16569) of nps exceeded the 45 × and 100 × thresholds, respectively. A similar distribution pattern was also observed in previous studies [31,32], and it did not change significantly among samples in this study.

In a more in-depth look at amplicon performance in Table S2 and Figure S2A–B, the average RD of 234 amplicons was 4500 ×, and the amplicon RD balance ranged from 0.01 for mt_106 (nps 7508–7590) to 10.20 for mt_221 (nps 15712–15788) with 73.93 % (173/234) amplicons > 0.20. Extremely low RD (amplicon balance < 0.05) was mainly identified in 13 amplicons marked in orange in Fig. 1, including mt_18 (nps 1094–1177), mt_64 (nps 4299–4379), mt_88 (nps 6109–6149), mt_98 (nps 6718–6810), mt_104 (nps 7256–7367), mt_106 (nps 7508–7590), mt_118 (nps 8290–8379), mt_178 (nps 12621–12683), mt_194 (nps 13657–13701), mt_204 (nps 14465–14532), mt_206 (nps 14609–14682), mt_208 (nps 14768–14809), and mt_214 (nps 15172–15213), occasionally in 5 amplicons marked in yellow in Fig. 1, including mt_54 (nps 3550–3606), mt_76 (nps 5307–5347), mt_85 (nps 5858–5975), mt_101 (nps 7021–7090), and mt_218 (nps 15519–15581). Four low-performing amplicons (mt_54, 98, 76, and 218) were also reported by Peng *et al.* [32], in which another two amplicons were not observed in our study: mt_5 (nps 267–347; amplicon RD balance = 0.70) and mt_177 (nps 12466–12614; amplicon RD balance = 0.32). Additionally, seven regions of amplicons (mt_54, 76, 194, 204, 206, 208, and 218) were flagged with low performance when using two long amplicons on the Ion Torrent PGM platform [5]. These particularly low RD regions were mainly located within tRNA (e.g., glutamine, aspartic acid, and lysine), NADH dehydrogenase, and Cytochrome b coding regions (Table S3). The features and structures inherited in the mtGenome are likely to be independent of sequencing strategies and platforms applied.

Interestingly, 88.89 % (16/18) of low-performing amplicons were concentrated in the WGS2. A comparison of the amplicon RD showed a statistically significant difference (W = 11594, $p < 2.20 \times 10^{-16}$, Wilcoxon rank sum test with continuity correction), i.e., WGS1 (odd-numbered amplicons; 6930 × ± 7353 ×) yielded about three times higher than WGS2 (even-numbered amplicons; 2070 × ± 4277 ×) as shown in Figure S3. However, the amplicon RD did not have a linear correlation with the amplicon length (F = 2.0510, $p = 0.1534$, F-statistic), and the coefficient of determination (adjusted R^2) demonstrated that the amplicon length only explained 0.45 % of the amplicon RD variation. This was also confirmed by Holt *et al.* [31]. The primer set imbalance may be explained by discrepancies in targeted PCR and bridge PCR on account of preferential amplification, as well as by stochastic factors or inconsistencies in manual library preparation, which were also observed in previous studies using the Precision ID mtDNA Whole Genome Panel on the Ion S5 platform [20,22,24,27,50].

3.2.2. Strand bias

The mean ± SD of #F/#R was calculated for SB as 1.04 ± 0.38 across 16569 nps. Also, the distribution plot in Fig. 1 showed fluctuations across the mtGenome, with more forward biases (54.25 % nps > 1) than reverse biases (45.75 % nps < 1).

Only 2.63 % (435/16569) of nps had a #F/#R value > 2.50 or < 0.40, namely a [1 − (#S/#L)] value > 0.60, which is a little higher than 1.68 % reported by Peng *et al.* [32]. The SB values were almost calculated as 0.00 between np 303 and np 347, indicating only reverse strand reads in this region, which was consistent with findings from previous studies [31,32]. It is explained by the fact that forward strand reads in this region do not meet alignment requirements due to the C-stretch, which is characterized by a variable number of consecutive cytosine (C) nucleotides. As a result, these forward strand reads are clipped by UAS [31].

In Table S2 and Figure S2C–D, the average value of #F/#R for the amplicon SB and [1 − (#S/#L)] for the amplicon SB balance across 234 amplicons was 1.03 and 0.05, respectively. The amplicon SB balance ranged from 0.00 for mt_134 (nps 9489–9526) to 0.87 for mt_88 (nps 6109–6149) with 2.14 % (5/234) amplicons > 0.60: mt_18 (nps 1094–1177), mt_23 (nps 1488–1532), mt_85 (nps 5858–5975), mt_86 (nps 5993–6023), and mt_88 (nps 6109–6149). Another 9 amplicons with a higher SB (amplicon balance > 0.20) are highlighted in purple in Fig. 1, such as mt_5 (nps 267–347), mt_60 (nps 3981–4028), mt_98 (nps 6718–6810), mt_101 (nps 7021–7090), mt_113 (nps 7960–8014), mt_191 (nps 13469–13511), mt_207 (nps 14686–14746), mt_216 (nps 15296–15358), and mt_234 (nps 16509–30). It was worth noting that the same five poorly performing amplicons (mt_18, 23, 88, 98, and 191) were also reported by Peng *et al.* [32]. However, unlike the amplicon RD, no statistically significant difference was found in comparing the amplicon SB between the two primer sets (W = 6676, $p = 0.7456$, Wilcoxon rank sum test with continuity correction). In addition, Fig. 1 displays the five most vulnerable amplicons, identified with low RD and high SB relative to the rest of the mtGenome: mt_18 (nps 1094–1177), mt_85 (nps 5858–5975), mt_88 (nps 6109–6149), mt_98 (nps 6718–6810), and mt_101 (nps 7021–7090). These regions may need to be reviewed manually, base by base, using visual software tools.

3.2.3. MtGenome coverage

The average percentage of mtGenome coverage was 99.95 % ± 0.15 %, with a range of 99.32 %–100.00 %. Of the 60 samples in this study, 52 (86.67 %) were observed with complete mtGenome coverage and 8 with amplicon dropouts due to mutations in primer-binding regions. This resulted in an on-target rate of 99.94 % (14032 out of 14040 targeted amplicons). Figure S4 shows primer-binding mutations and

MITOMAP frequencies in the following off-target amplicons: mt_2 (nps 108–146; 94A; 0.386 %), mt_43 (nps 2803–2850; 2887C; 0.296 %), mt_98 in two samples (nps 6718–6810; 6680C; 1.994 %), mt_104 (nps 7256–7367; 7245G; 0.072 %), mt_118 (nps 8290–8379; 8393T; 0.509 %), mt_194 (nps 13657–13701; 13722G; 0.739 %), and mt_229 (nps 16198–16241; 16271C; 0.676 %). Each of these mutations, except for 6680C, was not included in the kit design as they occur at < 1 % in the MITOMAP Database r107 (accessed May 24, 2024).

3.3. Tertiary data analysis

The average number of variants found in 60 samples was 40, ranging from 27 to 54. A total of 2426 variants were observed at 491 nps, where 2156 (88.87 %) were substitutions and 270 (11.13 %) were indels. Table S3 indicates that 760 (31.33 %), 1662 (68.51 %), and 4 (0.16 %) variants were observed in CR, gene-coding regions in CodR, and non-coding regions in CodR, respectively. The highest number of variants were observed in HVS-II (326 variants at 39 nps), Cyt b (304 variants at 43 nps), and HVS-I (285 variants at 68 nps). As expected, a high density of polymorphisms was observed with 721 (29.72 %) variants at 117 nps when combining HVS-I, HVS-II, and HVS-III. Fig. 1 illustrates the variant distribution against mitochondrial nps, where variants 73G, 263G, 315.1C, 750G, 1438G, 2706G, 4769G, 7028T, 8860G, 11719A, 14766T, and 15326G were observed from almost all samples (at least from 54 samples) and variants 489C, 8701G, 9540C, 10398G, 10400T, 10873C, 12705T, 14783C, 15043A, 15301A, and 16223T were observed from about half of the samples (at least from 30 samples). These high frequencies of variants were also observed in Northern Han Chinese except for 315.1C that was ignored in calculations [5]. Haplotypes and haplogroups in this study were approved by the EMPOP with the accession number EMP00881.

3.3.1. Substitutions

In terms of substitutions, 2074 transitions and 82 transversions were

Table 1
Insertions and deletions (indels) observed in this study (N = 60).

Region	rCRS	Indel	Manual inspection[a]	N	UAS (IT: >20 % for INS and >30 % for DEL)[b]	N	LHP
191	A	INS	191.1A	1	191.1A (99.9 %)	1	
247–249	GAA	DEL	249DEL	9	249DEL (100.0 %)	9	
283–291	A_2+C+A_6	DEL	285DEL	1	285DEL (100.0 %)	1	
303–309	C_7	INS	309.1C	20	309.1C (92.8 %)	11	
					309.1c (72.3 %)	5	Yes
					309.1C 309.2c (86.3 %; 29.8 %)	4	Yes
		INS	309.1C 309.2C	9	309.1C 309.2C (93.6 %; 83.1 %)	3	
					309.1C 309.2c (89.9 %; 67.2 %)	5	Yes
					309.1C 309.2c 309.3c (91.7 %; 71.7 %; 30.0 %)	1	Yes
311–315	C_6	INS	315.1C	57	315.1C (95.2 %)	57	
303–315	C_7+T + C_6	DEL/INS	**309DEL 315.1C**	2	309T 310C (100.0 %; 100.0 %)	2	
		DEL/INS	**309DEL 315.1C 315.2C**	1	308.1T 310C (92.7 %; 100.0 %)	1	
318–319	TT	INS	319.1T	1	319.1T (99.5 %)	1	
509–511	C_3	DEL	511DEL	1	511DEL (100.0 %)	1	
514–524	C+ $[AC]_5$	DEL	523–524DEL	27	523DEL 524DEL (84.0 %; 83.9 %)	27	
568–573	C_6	INS	573.1C 573.2C 573.3C 573.4C	2	573.1c 573.2c 573.3c 573.4c 573.5c (76.2 %; 76.2 %; 71.4 %; 57.1 %; 31.7 %)	1	Yes
					573.1C 573.2C 573.3C 573.4c (80.0 %; 90.0 %; 90.0 %; 60.0 %)	1	Yes
			573.1C 573.2C 573.3C	1	573.1C 573.2C 573.3c (86.8 %; 86.8 %; 51.5 %)	1	Yes
			573.1C 573.2C	1	568.1a 568.2c 573.1c 573.2c 573.3c (21.4 %; 21.4 %; 56.1 %; 57.9 %; 26.3 %)	1	Yes
			573.1C	1	573.1C (96.4 %)	1	
594–595	CC	INS	595.1C	1	595.1C (80.5 %)	1	
956–965	C_5+T + C_4	INS	960.1C 960.2C 960.3C 960.4C 960.5C	1	960.1C 960.2C 960.3c 960.4c 960.5c (80.2 %; 80.2 %; 79.9 %; 77.3 %; 53.6 %)	1	Yes
		INS	**960.1C**	4	[961C] 965.1c 965.2c (60.3 %; 28.7 %)	3	Yes
					[961C] 965.1c (53.7 %)	1	Yes
		DEL	960DEL	1	960DEL (100.0 %)	1	
2227–2232	A_6	INS	2232.1A	1	2232.1A (95.7 %)	1	
3168–3172	C_5	INS	3172.1C	3	3172.1C (95.6 %)	3	
5895–5899	C_5	INS	5899.1C	3	5899.1C (98.3 %)	2	
					5899.1c (77.1 %)	1	Yes
8271–8289	A+ $[C_5$+TCT+$A]_2$	DEL	**8281–8289DEL**	7	8271–8279DEL (92.6 %; 92.6 %; 92.6 %; 93.4 %; 92.6 %; 92.6 %; 93.6 %; 93.5 %; 92.5 %)	7	
15940–15944	T_5	DEL	15944DEL	1	15944DEL (100.0 %)	1	
16180–16193	A_4+C_5+T + C_4	DEL	**16193DEL**	5	16182C 16183c 16189C (81.9 %; 48.8 %; 89.9 %)	2	Yes
					16182C 16183c 16189C 16193c (100.0 %; 46.1 %; 100.0 %; 68.0 %)	1	Yes
					16182c 16183c 16189C (67.8 %; 44.6 %; 100.0 %)	1	Yes
					16182DEL 16183DEL 16186.1T 16189C (100.0 %; 100.0 %; 93.8 %; 100.0 %)	1	

INS: insertion; DEL: deletion; LHP: length heteroplasmy.

[a] The misalignment called by the Universal Analysis Software (UAS) is emphasized in bold.

[b] The ambiguous call code is used for the indel and a base call at a position exceeding the interpretation threshold (IT), and the average indel frequency is listed in the bracket, e.g., 309.1c (72.3 %) shows an ambiguous insertion occurring at position 309 with an insertion call (the average frequency of 72.3 %) and a reference call of C, as both frequencies are more than 20 % established for the insertion IT in this study.

observed with a 25.29:1 ratio of transitions to transversions, which was similar to the ratios of 20.89:1 in Northern Han Chinese [5] and 31.07:1 in Eastern Han Chinese [51]. The EMPCHECK tool detected 5 new transversions (A9596T, C9779G, A10963C, A11800T, and A14914C, shown in Figure S5) that are not included in the EMPOP v4/R13, but A9596T, A11800T, and A14914C can be found in the MITOMAP r107. Additionally, 12 unique PHPs were found: 6 in CR and 6 in CodR (discussed in Section 3.3.3). Furthermore, 4 tri-alleles (T9824A/C, G13928A/C, G15884A/C, and A16293C/G) were observed. All are included in the EMPOP and MITOMAP, and T9824A/C were reported in Northern and Southern Han Chinese [5,32]. Table S4 indicates no statistically significant differences in alternative allele frequencies between the dataset from this study and the other datasets (all $p > 0.05$, Proportion test) except for G13928A (this study *vs.* MITOMAP).

3.3.2. Insertions and deletions

Unlike substitutions, indels generally occur at a lower frequency in the mtGenome. A total of 132 insertions were detected, including 10 single-nucleotide insertions at nps 191 (191.1A), 319 (319.1T), 595 (595.1C), 2232 (2232.1A), 3172 (3172.1C), and 5899 (5899.1C), as well as 122 C_n insertions at nps 309 (309.XC), 315 (315.XC), 573 (573.XC), and 960 (960.XC). Additionally, 138 deletions were found at nps 249, 285, 309, 511, 523–524, 960, 8281–8289, 15944, and 16193. Two new indels (285DEL and 319.1T, shown in Figure S6) are not included in the EMPOP but in the MITOMAP.

The manual inspection of these 18 indel regions/positions in Table 1 revealed that UAS under the condition of customized ITs (>20 % for insertions and >30 % for deletions) and temporarily not considering LHPs (discussed in Section 3.3.3) correctly aligned 70.74 % (191/270) indels according to the ISFG guidelines [52] and misalignment was found in four regions. First, due to **C309DEL** existing, UAS misaligned its downstream nps towards the 5' end but not the 3' end, which resulted in C309T T310C C311–C315 in two samples and C308.1T C309 T310C C311–C315 in one sample (Figure S7). Second, a homopolymeric tract of 11 Cs occurred between nps 956 and 965 due to T961C and the insertion of a C. According to the phylogenetic rule, T961 C and 965.XC in two samples are diagnostic mutations for haplogroup A5b, while T961C and 965.XC in the other two samples are diagnostic and global private mutations for haplogroup N9a2. According to the forensic rule, indels should be placed at the 3' end unless the phylogeny suggests otherwise. Thus, UAS initially notated this region as T961C and 965.1C (Figure S8). However, EMPOP authenticated and revised them to **960.1C** and T961C according to the realigned PhyloTree Build 17 [53]. Third, UAS misaligned a 9-bp deletion towards the 5' end (8271–8279DEL in Figure S9) rather than the 3' end (**8281–8289DEL**) in all seven samples, which is not consistent with the forensic rule. Fourth, the most complicated region was located around nps 16182–16193, containing an uninterrupted stretch of 12 Cs and a heteroplasmic mixture of sequences due to the presence of A16182C A16183C T16189C. When C deletions emerged, similarly, UAS always misaligned them to np 16183, occasionally along with np 16182, but not to np **16193** (Figure S10). This region must be thoroughly inspected using IGV and then named according to the SWGDAM interpretation guidelines [54,55]. Most importantly, UAS only provides the universally user-defined IT (>10 % set in this study instead of the default >6 %). The lower IT makes it more challenging to interpret indels within or around homopolymers [5] and then determine the major molecule of LHP. It would be beneficial if UAS could offer separatable ITs, e.g., > 10 % for substitutions, > 20 % for insertions, and > 30 % for deletions, as recommended by Sturk-Andreaggi *et al.* [56] and defined in Converge from Thermo Fisher Scientific [27].

3.3.3. Heteroplasmy

With respect to PHPs, the minor allele frequency (MAF) > 10 % was utilized as IT. In cases of LHPs, the major molecule was reported according to the ISFG and SWGDAM guidelines [52,54].

A total of 22 potential PHP positions were listed in Table S5. Finally, the removal of mixtures at 10 positions was authenticated as follows: (1) PHP hotspots at nps 4048 (4/60), 4104 (4/60), 4456 (4/60), 5147 (3/60), 5580 (3/60), 8943 (3/60), 16444 (6/60), and 16496 (6/60) might be uncommon in a single population, and mixtures were actually caused by NUMT intrusions from HSA_NumtS_001_b1 (hg19 chr1:564465–570304) and HSA_NumtS_587_b1 (HE613849.1) that were identified using the BLAST. Although UAS had been developed to eliminate potential mixtures and thereby could authenticate PHPs, NUMTs still bleed through in some instances, especially when a sample had low quality using the short amplicon method. (2) mixtures at nps 8104 and 14720 violating the double-strand confirmation (i.e., observation of the variant nucleotide in sequences from both directions [57]), where 8104G and 14720G were only observed on the reverse strands. Interestingly, mixtures at np 8104 might be caused by misalignment owing to 8281–8289DEL at the end of this amplicon. Hence, any PHP should be carefully interpreted by referring to raw data or confirmed by Sanger sequencing if necessary. Finally, 12 PHPs were observed among 11 individuals, accounting for 18.33 % (11/60) of the individuals studied (Figure S11). One individual presented two PHPs (8812R and 16086Y). Each position appeared to be heteroplasmic in only a single individual. Concerning the type of PHPs, five were purine transitions, and seven were pyrimidine transitions, but no transversion was detected. The PHP distribution showed a frequency of 50 % was observed in the CR and 50 % in the CodR (16.67 % in tRNAs and 33.33 % in protein-coding gene positions), which was lower than 61.45 %–84.38 % of PHPs in the CodR in previous observations [5–7,24,32,58–61]. In the CR, 16093Y has often been observed as a hotspot [5,57] with a high frequency indexed in the EMPOP (299 hits in 48572 mitogenomes). Additionally, 207R, 235R, 16086Y, 16124Y, and 16201Y were observed in the EMPOP. In the CodR, five PHPs (7028Y, 8812R, 12311Y, 13038Y, and 14693R) in our study were unique, and 8784R could be observed in the EMPOP (1 hit in 4471 mitogenomes). This randomly distributed pattern of PHPs in the CodR was also observed in previous studies [5,32,57].

LHP is believed to occur due to polymerase slippage during DNA replication, which is often observed when there are seven or more consecutive cytosines (Cs) within C-stretches [56]. Additionally, LHP is usually found due to stutters of $[AC]_n$ in nps 515–524 and $[C_5+TCT+A]_n$ in nps 8272–8289 [57]. In this study, half of the individuals (30/60) exhibited LHPs using insertion IT > 20 % and deletion IT > 30 %. A total of 24 individuals had only one LHP, while the remaining individuals carried more than one LHP. The observed ranges of LHPs were found in nps 303–309 (8–9 Cs), 568–573 (8–10 Cs), 956–965 (10–11 Cs), 5895–5899 (6 Cs), and 16182–16193 (7–12 Cs). Table S6 indicates that 83.33 % (30/36) of LHPs and 45.00 % (26/60) of samples were observed in the common C-stretches of the CR, with the highest frequency (25.00 %; 15/60) located in nps 303–309 and the second highest (18.33 %; 11/60) in nps 16182–16193. These LHP hot ranges in HVS-II and HVS-I have also been reported in previous studies [5,56,58,62]. Contrasting with earlier research [5,25,58], LHP in nps 311–315 was not observed in this study and Peng *et al.* [32]. Similarly, LHPs in nps 515–524 and 8272–8289 were not observed here but were reported by Peng *et al.* [32] using the default deletion IT (>6 %). These results can differ based on the enrichment methods, sequencing chemistries or platforms, and analysis software or workflows.

3.4. Internal validations

Internal validations are intended to demonstrate that established methods and procedures perform as expected for forensic applications in our MPS laboratory, including sensitivity, repeatability, concordance, degraded samples, inhibitor samples, case-type samples, and contamination assessment in this study. Fig. 2 shows the number of reads (intensity) and read distribution for each sample (Run 1–4).

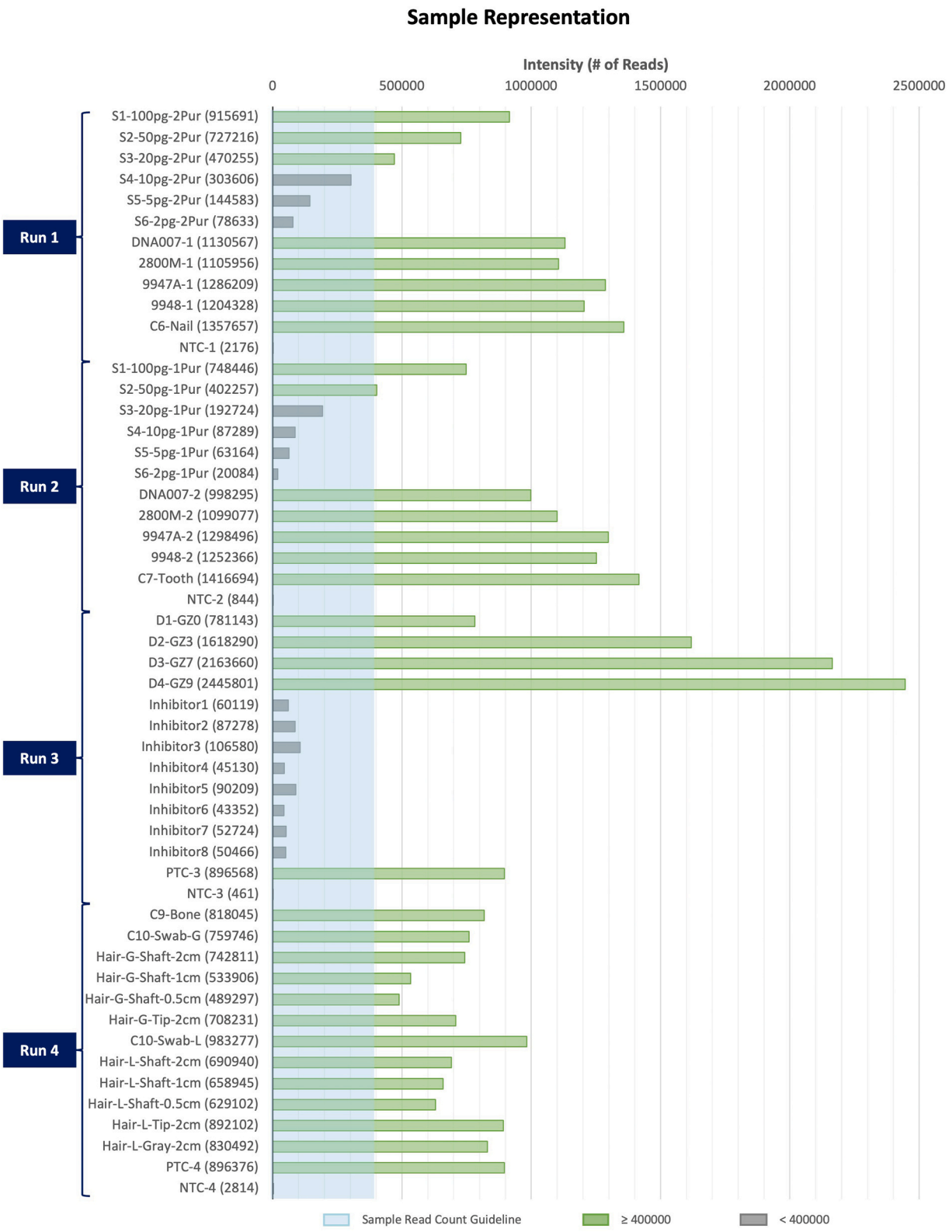

Fig. 2. Sample intensity in internal validations. The vertical light blue area represents the minimum number of reads (400000 ×) recommended for a given sample. The bar graph illustrates the total reads from the associated sample in Run 1–4, where the read count is depicted as ≥ 400000 × in green and < 400000 × in grey.

3.4.1. *Sensitivity*

Sensitivity studies were conducted with the HL60 gDNA at various input levels: 100 pg, 50 pg, 20 pg, 10 pg, 5 pg, and 2 pg. The studies were performed twice: once using two rounds of bead purification (sample intensity shown in Run 1 in Fig. 2 and average RD per np represented by the dark green bars in Figure S12) and once with one round of bead purification (sample intensity shown in Run 2 in Fig. 2 and average RD per np represented by the light green bars in Figure S12). It indicates that two rounds of purification followed by the bead-based normalization (BBN) method can improve data recovery

from the mtGenome for samples with an input of 20 pg gDNA or less (intensity >100 % increases and average RD >150 % increases in Table S7). This improvement was also observed in the developmental validation studies between two rounds of purification followed by the manual quantification normalization (QN) and one round of purification followed by the BBN [31]. As expected, Figure S12 illustrates the average RD declined with each reduction in the gDNA input amount. Additionally, the percentage of the mtGenome coverage was 100 % at each amount with two rounds of purification. However, gaps appeared in the mtGenome with one round of purification when the amount decreased to 5 pg (mt_106 and mt_204 dropouts) and 2 pg (mt_18, 98, 106, and 204 dropouts). These low-performing amplicons were identified in Section 3.2.1. Fortunately, all 35 expected variants (34 substitutions and one insertion) for HL60 were obtained at each amount, and thus the haplogroup assignment was accurately estimated. Further, the percent C at 315.1C, T2445Y, and T12071Y in the *Sample Report* were compared, revealing no significant differences between one and two rounds of bead purification (all $p < 0.05$, one-way ANOVA). Thus, the average proportions were calculated as 80.28 % ± 5.03 % for reference allele T and 19.72 % ± 5.03 % for alternative allele C at 2445Y and 48.39 % ± 7.89 % for reference allele T and 51.61 % ± 7.89 % for alternative allele C at 12071Y. The results observed were comparable to those of 2445Y (T: 84.70 %; C: 15.30 %) and 12071Y (T: 48.50 %; C: 51.50 %) as reported by Cihlar *et al.* [50]. Additionally, they were similar to 12071Y (T: 50.44 %; C: 49.56 %) reported by Riman *et al.* [63], but differed from the results for 2445Y (T: 92.25 %; C: 7.63 %). The conclusion reached by Cihlar *et al.* [50] may be associated with the use of cell lines from differing lots.

3.4.2. Repeatability and concordance

Repeatability studies were performed by sequencing five control DNA libraries (HL60, DNA007, 2800M, 9947A, and 9948) in two separate runs on the same MiSeq FGx instrument by the same operator. The one-way ANOVA results showed no significant differences between the two runs in sample intensity ($p = 0.6835$), average RD ($p = 0.4042$), average amplicon RD ($p = 0.4707$), or average #F/#R ratio ($p = 0.4153$). Precision was measured by the percentage of the mtGenome coverage [31]. The results demonstrated 100 % precision for the mtGenome, and consistent variants from five control samples were identified in two separate runs. The pairwise difference of variant frequency (variant reads divided by total reads at a variant position) for each variant in each sample between two runs was 0.00 % for substitutions, 2.32 % ± 2.42 % for PHPs, and 1.33 % ± 1.50 % for insertions and mixed insertions, respectively. The maximum difference was observed at 2445Y from HL60 (6.24 %) and 573.3C from DNA007 (4.75 %), respectively, which was similar to the proportions of mixed bases (9.60 %) and length and mixed length regions (3.30 %) reported in developmental validation studies [31]. Additionally, the PTCs (HL60) from different lots were evaluated. The data showed that 32 consistent substitutions and one insertion were observed in the HL60 across 9 runs in this study and previous studies [31,32,50,63]. However, two positions involving PHPs (IT > 10 %) exhibited variability (Figure S13). At np 2445, the reference allele T was recorded in [32,63] and in Run 4, 7, and 9 with the alternative allele C frequency of 0.0 % inspected using IGV, while 2445Y was called in [31,50] and in other runs (C: 20.83 % ± 2.74 %). Similarly, T12071 was observed in [32] and the same runs (4, 7, and 9) with the alternative allele C frequency of 1.0 %, but other studies [31,50,63] and other runs (C: 50.53 % ± 1.71 %) in this study identified it as 12071Y. As discussed in Section 3.4.1, it was explained by lot-to-lot variation [50] and also observed in the example run from the UAS server (Figure S13).

The haplotypes from the five control DNA samples included in concordance studies are detailed in Table S8. The variants for DNA007 showed concordance with 35 substitutions and 5 insertions previously reported using the Ion S5 sequencer [27,50], with the exception of three heteroplasmic positions: 1420, 1599, and 2413. The 1420Y was identified in duplicate with an average frequency of alternative allele C at 20.4 %, but T1420 was referenced in [27,50]. In contrast, the 1559R was reported in [27], while A1559 was called in this study as well as in [50] with an average G frequency of 7.7 %. The 2413Y was also called in duplicate with an average T frequency of 15.06 %. However, C2413 was reported in [27] and in [50] with 4.9 %. The haplotypes for 2800M and 9947A were fully concordant with those reported by Cihlar *et al.* [50]. For 9948 Male DNA, 34 substitutions matched those reported by Chen *et al.* [14], but two insertions (309.1C and 315.1C) were missing using that nanoball sequencing platform. Repeatability and consistency studies have shown that PHPs are most prone to discordance for control DNA samples, followed by LHPs, which vary in sequencing platforms/chemistries, analysis software/interpretation thresholds, and lots of cell lines [50].

3.4.3. Degraded samples

Degraded samples were obtained with 29 identical variants (27 substitutions, one deletion, and one insertion) and assigned to haplogroup F2d, with 0.71 (PTC), 4.52 (Day 3), 63.84 (Day 6), and 146.01 (Day 9) DI. Interestingly, the concentration of purified mtGenome libraries (listed in Table 2) and the number of reads (shown in Run 3 in Fig. 2) were progressively generated with DI increased. This may be due to the method used to quantify gDNA to infer mtGenome content (50 pg gDNA ~ 6000 mtGenome copies [12]). The Quantifiler® Trio DNA Quantification Kit is designed to amplify and detect the human-specific target loci, which consist of multiple copies dispersed on various autosomal chromosomes, known as the Small Autosomal (SA; 80 bp) and Large Autosomal (LA; 214 bp) targets, and male-specific multiple copies on the Y-chromosome, known as the Y targets (75 bp) [38]. The primary quantification targets (SA and Y) are utilized to detect degraded samples. DI refers to the data observed when a sample shows a reduction in the measured amount for LA compared to SA, i.e., DI = SA concentration / LA concentration [38]. Thus, mtGenomes were input more than expected because they may be less degraded than nuclear genomes, as also observed in aged bones reported by Obal *et al.* [64]. Although > 0.99 of average #F/#R ratio and 100 % of mtGenome coverage were achieved from all samples, the number of low-performing amplicons (specifically mt_85 from Day 6 and mt_18, 85, 101, and 106 from Day 9) and artificial heteroplasmic positions (np 247 from Day 6 and nps 247 and 1041 from Day 9) was incrementally observed with DI increased. Table 2 shows the number of variants/alleles and the percentage of profiles of degraded samples obtained using the ForenSeq™ mtDNA Whole Genome Kit and MPS/CE A/Y-STR kits [65,66]. Clearly, the mtGenome assay proved to be more advantageous for severely degraded samples (DI >10) and was found to be superior to the MPS A/Y-STR kits, which in turn were better than the CE-A/Y-STR kits. This has been discussed in previous studies [65,66].

3.4.4. Inhibitor samples

Hematin has been identified as a PCR inhibitor in samples. It is co-extracted and co-purified with DNA and subsequently interferes with PCR by inhibiting the activity of polymerase [67]. Fig. 3A shows that the input DNA amount from inhibitor samples, along with other samples in Run 3, was added at 100 pg into targeted PCR amplification. However, the average concentration of mtGenome libraries for inhibitor samples was only 0.65 ng/μL after two rounds of purification, which was sharply decreasing compared to the PTC sample (Fig. 3B). Without doubt, the sample intensity of inhibitor samples averaged 0.067 M reads, far lower than the recommended minimum number of reads (0.4 M), and so did the average RD (560 ×) in Fig. 3C, which was only one-tenth of the reads reported in Section 3.2.1. It indicates that the Automatic 96 Channel Micro DNA Extraction Workstation did not remove the inhibitors well, thereby affecting the downstream workflow. As shown in Figure S14, the CE results can also confirm this speculation. Further, the same inhibitor samples were processed for extraction and purification on the AutoMate Express™ Forensic DNA Extraction System, resulting in a

Table 2
The number of variants (or alleles) and the percentage of coverages (or profiles) recovered from degraded samples with the ForenSeq ™ mtDNA Whole Genome Kit and other autosomal/Y-chromosomal STR kits.

Sample	Degradation Index	Concentration (ng/μL)	Mitochondrial DNA					Nuclear DNA [64,65]									
			Input gDNA (ng)	Purified library (ng/μL)	ForenSeq mtDNA Whole Genome Kit				Input gDNA (ng)	Precision ID Globalfiler NGS STR Panel v2		GrandFiler Y-STR Panel		PowerPlex 21 System		Yfiler Platinum Casework PCR Amplification Kit	
					# of Variant	% of Coverage	# of Position	% of Coverage		# of Allele	% of Profile	# of Allele	% of Profile	# of Allele	% of Profile	# of Allele	% of Profile
Control	0.71	7.82	0.1	2.5	29	100.00	16569	100.00	1	55	100.00	104	100.00	35	100.00	41	100.00
Day 3	4.52	2.82	0.1	14.4	29	100.00	16569	100.00	1	55	100.00	93	89.42	33	94.29	40	97.56
Day 6	63.84	0.14	0.1	48.5	29	100.00	16569	100.00	1	52	94.55	83	79.81	18	51.43	23	56.10
Day 9	146.01	0.02	0.1	> 55.0	29	100.00	16569	100.00	0.3	52	94.55	67	64.42	10	28.57	11	26.83

three-fold increase in the final concentration of purified mtGenome libraries (data not shown). Additionally, samples with high levels of inhibitors cannot only negatively affect targeted PCR amplification of their own DNA but also potentially inhibit cluster generation and sequencing [68]. Quality metrics for Run 3 in UAS were within the recommended range, except for phasing (> 0.25 % in Figure S15). This suggests that the efficiency of sequencing synthetase is reduced, which is common in the case of outdated reagents and pooled libraries containing too many inhibitors [68].

3.4.5. *Case-type samples*

The analyses of mtGenome for blood and muscle samples have been presented in Sections 3.2–3.3 and 3.4.3, respectively. Five other types of samples (nail, tooth, bone, buccal swab, and hair shaft) were also examined (Table S9 and Fig. 2).

For the nail sample, the quantified concentration of gDNA was 3 pg/μL; thus, only 36 pg of input gDNA (18 pg each for WGS1 and WGS2) could be added during the library preparation. This amount is below the minimum requirement of 100 pg for both CE and MPS assays needed to obtain complete STR and/or SNP profiles [65,66,68–70]. In earlier studies, incomplete profiles with 15, 60, and 87 alleles were explored from the same nail at 45 pg of input gDNA using the PowerPlex® 21 System, Precision ID Globalfiler™ NGS STR Panel v2 [65], and GrandFiler Y-STR Panel [66], respectively. Despite this, the average RD (13383 ×) and SB (0.9952) across 16569 positions for the nail were comparable to those for other samples in the same run. No loss of mtGenome coverage was observed, and 45 variants (41 substitutions, three insertions, and one deletion) were identified and assigned to haplogroup Z3d, which aligns with the genetic background of the East Asian population [46].

This issue was also noted in the severely degraded tooth sample (DI = 11.21), for which only 72 pg of input gDNA (36 pg each) could be added maximally. This amount also falls below the minimum requirement of 100 pg. Only 10–26 alleles were unearthed using CE/MPS A-STR kits [65]. The comparable average RD and SB were obtained across the mtGenome, with two low-performing amplicons (mt_85 and mt_101 identified in Section 3.3.2). The percentage of mtGenome coverage was 99.43 %, with two amplicon dropouts due to 1–2 mutations in primer-binding regions (Figure S16). The first dropout was the mt_141 (nps 9999–10048), which was associated with a rare mutation 9968T (a frequency of 0.098 % in MITOMAP) in the upstream primer-binding region. The second dropout occurred in the mt_229 (nps 16198–16241), resulting from two mutations, 16261T with 7.066 % frequency and 16270T with 4.961 % frequency, in the downstream primer-binding region. Although two mutations occur at > 1 % in the MITOMAP, the manufacturer only designs the degenerate primers for np 16261 but not np 16270. In total, 19 substitutions, three insertions, and 11 deletions were identified and assigned to haplogroup B4g1a, while more irreproducible mixed bases not at diagnostic sites were observed than expected, such as 2378Y, 6482Y, 8215Y, and 9922Y. Those mixed bases may be caused by cytosine deamination in severely degraded samples [71].

Fortunately, although the bone sample was moderately degraded (DI = 7.31), the concentration of gDNA was measured at 26 pg/μL. At the recommended amount of input gDNA, 100 % of mtGenome coverage and 37 variants were achieved. Although this study had limited data, the results indicate that the ForenSeq™ mtDNA Whole Genome Kit is effective for detecting trace samples and/or severely degraded samples in real scenarios.

Most importantly, hair shafts and shed hairs without follicular tissue represent one of the most commonly encountered sample types in various cases, which often have limited DNA quantity and quality [12]. Hair shaft samples were prepared according to the procedures outlined in Section 2.1.6. As illustrated in Fig. 2 and Fig. 4, both the sample intensity and the average RD decreased as the segment length was reduced. Meanwhile, an increase in poorly performing amplicons

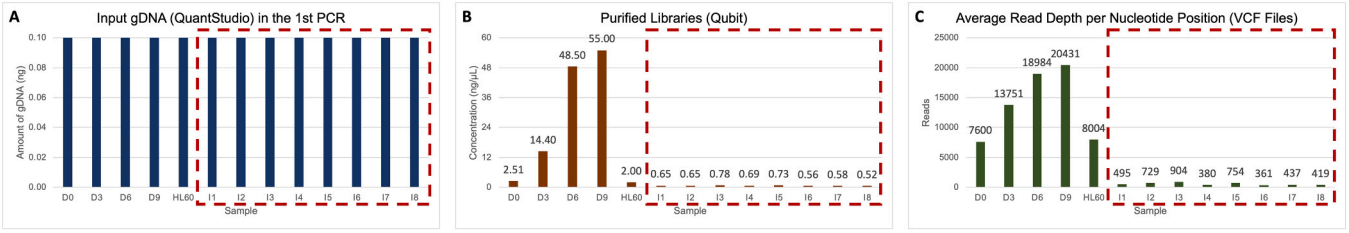

Fig. 3. Inhibitor samples. Subgraphs are plotted against four degraded samples, one positive control, and eight inhibitor samples in Run 3. (A) The amount of genomic DNA (gDNA) input into the targeted PCR is quantified using the Quantifiler® Trio DNA Quantification Kit on the Applied Biosystems® QuantStudio 5 Real-time PCR System. (B) The concentration of libraries following two rounds of purification is measured with the Qubit™ dsDNA HS Assay Kit on the Qubit™ 4.0 Fluorometer. (C) The average read depth per nucleotide position (np) is determined by summing all reads from a Variant Call Format (VCF) file and dividing the total by 16569 nps.

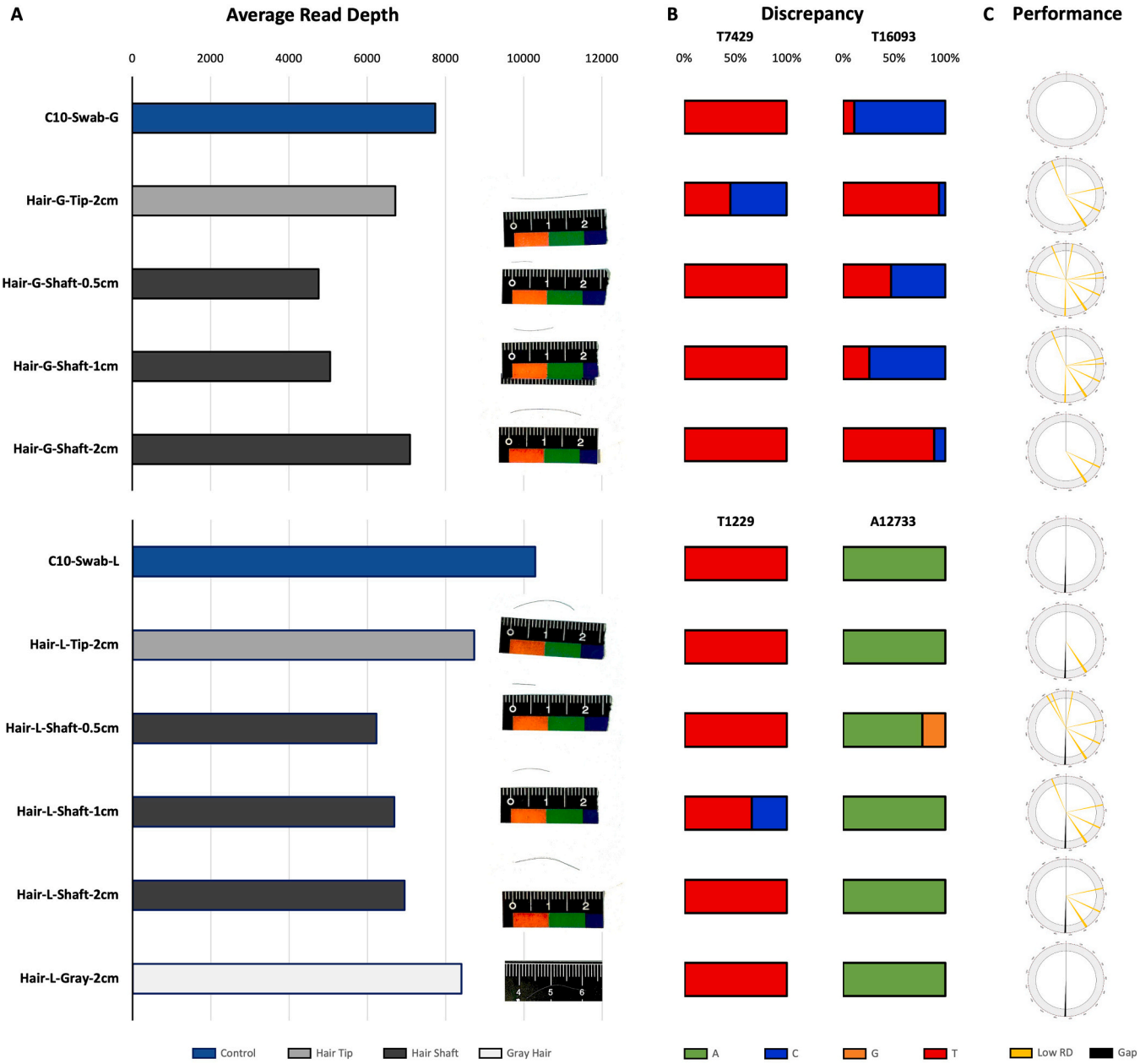

Fig. 4. Hair shaft and buccal samples. Group 1 consists of four undyed hair shafts (2 cm, 1 cm, and 0.5 cm from the root; 2 cm from the tip) collected from sample G along with one buccal swab. Group 2 comprises four undyed hair shafts (2 cm, 1 cm, and 0.5 cm from the root; 2 cm from the tip) and one grey hair shaft (2 cm from the root) obtained from sample L as well as one buccal swab. (A) The bar graph illustrates the average read depth at each nucleotide position. To the right, the corresponding specimen collected is presented with a ruler below. (B) The 100 % stacked bar shows the discrepancy and its variant frequency observed at a particular position among buccal and hair shaft samples. (C). A Circos plot displays the distribution of low-performing amplicons and/or gaps in a sample.

(yellow regions marked in Fig. 4) was noted with the length shortened. This observation is consistent with the expectation that as more hair shaft is extracted, more mtDNA is recovered [72]. In a comparative analysis of the RD for 234 amplicons obtained from 2 cm proximal and 2 cm distal hair shafts, it was determined that there were no statistically significant differences observed in sample G ($p = 0.8011$, one-way ANOVA) and sample L ($p = 0.2632$, one-way ANOVA). Similarly, no statistically significant difference was found between 2 cm undyed and gray proximal hair shafts in sample L ($p = 0.3033$, one-way ANOVA). Previous systematic studies have demonstrated that mtDNA quantity and quality decline distally from the root end of a hair [73]. However, the limited data in this study indicates that the location and state of the hair shafts sampled have little effect on the RD when using the ForenSeq™ mtDNA Whole Genome Kit. Compared with the buccal swab for sample G, the mtGenome coverage for all hair shafts was 100 %, and 35 identical variants (32 substitutions, two insertions, and one deletion) were identified and assigned to haplogroup F2a. Among substitutions, the heteroplasmic variant 16093Y is a PHP hotspot with the frequency of alternative allele C ranging from 6.00 % to 89.23 %, as illustrated in Fig. 4. Notably, mixed bases were detected in the hair tip (1227Y), while they were absent in the other samples (T1227). In sample L, all buccal and hair shaft samples yielded 99.46 % of mtGenome coverage, along with a consistent amplicon mt_118 dropout (nps 8285–8390). This occurrence was attributed to a rare primer-binding mutation 8392A, with a frequency of 0.705 % in MITOMAP (Figure S17). Consequently, 31 identical variants (29 substitutions and two insertions) were explored, while two additional mixed bases were encountered: 1229Y in the 1 cm half shaft and 12733R in the 0.5 cm half shaft. Nevertheless, these discrepancies did not affect the assignment of all samples into haplogroup Y1b1. True PHPs can be observed in a single hair or among hairs in a single individual [74]. Additionally, low-frequency variants in heteroplasmic sites may arise from NUMTs, mega-NUMTs, mixtures, cytosine deamination, and stochastic/sequencing errors [71].

3.4.6. Contamination assessment

The NTC should be evaluated for the presence of exogenous DNA that may come from reagents, consumables, other samples, the operator, and/or the laboratory environment [36]. The outcomes are presented in Table S10 for nine NTCs that were prepared along with other samples in Run 1–9. On average, 64 bases were covered using the default settings. Of these NTCs, six showed no reads across the mtGenome, while three NTCs exhibited detectable regions (two regions in Run 5 and three regions in Run 4&7) that ranged from 155 to 227 total bases. The average RD in the covered regions across these three NTCs varied from 64 × for the two regions of 155 bases to 114 × for the three regions of 227 bases. Furthermore, two variants were called: 11467G (RD: 123 ×) for NTC-4 and 3492G (RD: 84 ×) for NTC-7. A comparative analysis was conducted between these two NTC variants and the variants and mixed bases (below the 10 % interpretation threshold) from all samples and operators involved in this study; however, no overlaps were identified. Also, 3492G was not indexed in the EMPOP, and 11467G was not reported in the East Asian population. Figure S18A illustrates the distribution of the relative RD, defined as the ratio of RD for the NTC compared to the PTC within the same run at each np [27]. The average relative RD for NTCs was 0.0124 % ± 0.1384 %, markedly below the 6 % analytical threshold. Interestingly, the background noise in NTCs was relatively cleaner when employing two rounds of purification (e.g., Run 3&4) than one round (e.g., Run 5, 7&9), as depicted in Figure S18B. This observation further suggests that a second purification is highly beneficial for the amplified libraries to remove other reaction components. However, the stochastic base/variant calling encountered in the NTCs is a challenging phenomenon to circumvent, arising from the inevitable incorporation of aerosols during the pipetting process, the high sensitivity of the ForenSeq™ mtDNA Whole Genome Kit, and the occurrence of bioinformatic errors, which have also been reported in previous studies [27,31–33]. Fortunately, these contaminations in NTCs did not interfere with the mitochondrial analyses in this study.

4. Conclusion

The article delineates the workflow of library preparation utilizing the ForenSeq™ mtDNA Whole Genome Kit, as well as clustering and sequencing conducted on the MiSeq FGx® Sequencing System, followed by data analysis employing the UAS. Additionally, we assess its MPS performance across 9 consecutive runs and conduct internal validations in accordance with the SWGDAM guidelines. The workflow demonstrates proficient run metrics and MPS performance when 12–14 libraries are sequenced within a standard flow cell, including > 80 % of reads passing filter, > 80 % bases with ≥Q30, > 5000 × of the average RD at nps, ~1.0 of the average forward/reverse SB, > 70 % of the inter-amplicon balance, and > 99 % of the mtGenome coverage. Furthermore, the internal validations reveal favorable outcomes. Specifically, the workflow can produce repeatable and reproducible results, generate complete mtGenome profiles from ≥ 2 pg input gDNA for high quality samples/control DNA or ≥ 0.5 cm hair shafts, and recover more/complete mtGenome information from severely degraded samples (DI >10) and various types of case samples. Overall, the ForenSeq™ mtDNA Whole Genome Kit, including 234 short overlapping amplicons with an average size of 131 bp, can meet forensic needs on the whole mtGenome sequencing in real scenarios.

In addition, this study brings some experiences on the utilization of the ForenSeq™ mtDNA Whole Genome Kit. (1) DNA extraction and purification: An appropriate workstation should be employed for the lysis of mitochondrial organelles and removal of potential inhibitors, such as the AutoMate Express™ Forensic DNA Extraction System instead of the Automatic 96 Channel Micro DNA Extraction Workstation in Section 3.4.4. (2) DNA quantification: The method used for quantifying gDNA to infer mtGenome content may underestimate the actual mtGenome copies, particularly within severely degraded samples (Section 3.4.3). (3) Purify libraries: Conducting two rounds of purification can more effectively remove additional reaction components (Section 3.4.6) and enhance data recovery from the mtGenome, especially for low-input samples (Section 3.4.1). (4) Denature and dilute libraries: The pooled libraries can be more easily transferred and more fully denatured by adhering to the procedures outlined in the ForenSeq™ DNA Signature Prep Kit User Guide (Section 2.3). (5) Primer set imbalance: The amplicon RD for WGS1 is significantly higher than that for WGS2 (Section 3.2.1), which has also been observed in other manufacturers' kits. Whether or not to change the WGS1/WGS2 ratio necessitates further internal validation; however, it was not adjusted in this study. (6) Low-performing amplicons: The five most vulnerable amplicons exhibiting low RD and high SB are identified in Section 3.2.2, such as mt_18 (nps 1094–1177), mt_85 (nps 5858–5975), mt_88 (nps 6109–6149), mt_98 (nps 6718–6810), and mt_101 (nps 7021–7090), and those highly occurred in internal validations. An updated Verogen mtDNA Whole Genome V2 Analysis Method is introduced in UAS v2.6.0 or later, which improves the NUMT filter to prevent incorrect filtering of reads aligning to the mtGenome and facilitates the recovery of samples reads that align to the nuclear genome but have higher mapping to the mtGenome. Perhaps low-performing amplicons will be improved using the new analysis method. (7) Primer-binding mutation: Although the manufacturer has addressed known variants located in primer-binding regions, specifically those with > 1 % frequencies documented in MITOMAP, in instances where the mtGenome is not completely covered, the presence of rare mutations needs to be considered (examples in Sections 3.2.3 and 3.4.5). (8) Manual inspection: The overwhelming substitutions are accurately reported by UAS (Section 3.3.1), while indels, PHPs, and/or LHPs still need to be manually checked (Sections 3.3.2 and 3.3.3). First, UAS cannot provide separable interpretation thresholds, e.g., > 10 % for substitutions, > 20 % for insertions, and > 30 % for deletions, and it does not consider the major molecule rule reported for LHPs. Second, UAS edits the BAM files and Sample reports

for commonly observed indels according to the forensic rule but overlooks 8281–8289DEL. Third, the most complex region (nps 16182–16193) unequivocally needs manual inspection. (9) Lot-to-lot variation of PTCs: Despite utilizing the HL60 inside different lot-number kits provided by Qiagen, discordance can still be observed at positions involving PHPs (Section 3.4.2). (10) Contamination: Even though we do our best to avoid contamination with exogenous DNA throughout the process, the NTCs in certain runs still cover some reads (Section 3.4.6). These experiences may not always be comprehensive due to the limited sample size. We aspire to furnish helpful information for forensic laboratories considering implementing the ForenSeq™ mtDNA Whole Genome Kit.

CRediT authorship contribution statement

Yu Shaobo: Supervision, Conceptualization. **Zhang Biao:** Investigation. **Liu Ze:** Data curation. **Xuan Jinfeng:** Writing – original draft, Validation. **Wu Haiduo:** Methodology. **Long Guannan:** Validation, Methodology. **Guo Fei:** Writing – review & editing, Data curation, Conceptualization. **Ren Fu:** Writing – review & editing, Funding acquisition.

Declaration of Competing Interest

The authors declare that they have no known competing financial interests or personal relationships that could have appeared to influence the work reported in this paper.

Acknowledgments

This work was supported by the Team Construction Project of Liaoning Province Education Department under Grant LJ222410164013. The authors thank Ziming Deng at TopScience and Sheng Peng, Xiang Sheng, and Huiyuan Niu at QIAGEN for their technical support. Special thanks to the EMPOP team, represented by Walther Parson, for their advice and efforts in data quality control.

Appendix A. Supporting information

Supplementary data associated with this article can be found in the online version at doi:10.1016/j.fsigen.2025.103274.

References

[1] J.M. Butler, Advanced Topics in Forensic DNA Typing: Methodology, Academic Press, Boston, 2011.
[2] C. Yan, X. Duanmu, L. Zeng, B. Liu, Z. Song, Mitochondrial DNA: distribution, mutations, and elimination, Cells 8 (2019) 379, https://doi.org/10.3390/cells8040379.
[3] J.A. Irwin, J.L. Saunier, P. Beh, K.M. Strouss, C.D. Paintner, T.J. Parsons, Mitochondrial DNA control region variation in a population sample from Hong Kong, China, Forensic Sci. Int. Genet. 3 (2009) e119–125, https://doi.org/10.1016/j.fsigen.2008.10.008.
[4] W. Parson, C. Strobl, G. Huber, B. Zimmermann, S.M. Gomes, L. Souto, L. Fendt, R. Delport, R. Langit, S. Wootton, R. Lagacé, J. Irwin, Reprint of: evaluation of next generation mtGenome sequencing using the Ion Torrent Personal Genome Machine (PGM), Forensic Sci. Int. Genet. 7 (2013) 632–639, https://doi.org/10.1016/j.fsigen.2013.09.007.
[5] Y. Zhou, F. Guo, J. Yu, F. Liu, J. Zhao, H. Shen, B. Zhao, F. Jia, Z. Sun, H. Song, X. Jiang, Strategies for complete mitochondrial genome sequencing on Ion Torrent PGM™ platform in forensic sciences, Forensic Sci. Int. Genet. 22 (2016) 11–21, https://doi.org/10.1016/j.fsigen.2016.01.004.
[6] K. Ma, H. Li, Y. Cao, X. Zhao, W. Liu, X. Zhao, Haplotype diversity in mitochondrial genome in a Chinese Han population, J. Hum. Genet. 61 (2016) 903–906, https://doi.org/10.1038/jhg.2016.74.
[7] J.L. King, B.L. LaRue, N.M. Novroski, M. Stoljarova, S.B. Seo, X. Zeng, D. H. Warshauer, C.P. Davis, W. Parson, A. Sajantila, B. Budowle, High-quality and high-throughput massively parallel sequencing of the human mitochondrial genome using the Illumina MiSeq, Forensic Sci. Int. Genet. 12 (2014) 128–135, https://doi.org/10.1016/j.fsigen.2014.06.001.
[8] J.A. McElhoe, M.M. Holland, K.D. Makova, M.S. Su, I.M. Paul, C.H. Baker, S. A. Faith, B. Young, Development and assessment of an optimized next-generation DNA sequencing approach for the mtgenome using the Illumina MiSeq, Forensic Sci. Int. Genet. 13 (2014) 20–29, https://doi.org/10.1016/j.fsigen.2014.05.007.
[9] M.A. Peck, M.D. Brandhagen, C. Marshall, T.M. Diegoli, J.A. Irwin, K. Sturk-Andreaggi, Concordance and reproducibility of a next generation mtGenome sequencing method for high-quality samples using the Illumina MiSeq, Forensic Sci. Int. Genet. 24 (2016) 103–111, https://doi.org/10.1016/j.fsigen.2016.06.003.
[10] M.A. Peck, K. Sturk-Andreaggi, J.T. Thomas, R.S. Oliver, S. Barritt-Ross, C. Marshall, Developmental validation of a Nextera XT mitogenome Illumina MiSeq sequencing method for high-quality samples, Forensic Sci. Int. Genet. 34 (2018) 25–36, https://doi.org/10.1016/j.fsigen.2018.01.004.
[11] V. Sukser, F. Rokić, L. Barbarić, M. Korolija, Assessment of Illumina® Human mtDNA Genome assay: workflow evaluation with development of analysis and interpretation guidelines, Int. J. Leg. Med. 135 (2021) 1161–1178, https://doi.org/10.1007/s00414-021-02508-z.
[12] W. Parson, G. Huber, L. Moreno, M.B. Madel, M.D. Brandhagen, S. Nagl, C. Xavier, M. Eduardoff, T.C. Callaghan, J.A. Irwin, Massively parallel sequencing of complete mitochondrial genomes from hair shaft samples, Forensic Sci. Int. Genet. 15 (2015) 8–15, https://doi.org/10.1016/j.fsigen.2014.11.009.
[13] M. Mikkelsen, R. Frank-Hansen, A.J. Hansen, N. Morling, Massively parallel pyrosequencing of the mitochondrial genome with the 454 methodology in forensic genetics, Forensic Sci. Int. Genet. 12 (2014) 30–37, https://doi.org/10.1016/j.fsigen.2014.03.014.
[14] M. Chen, C. Chen, N. Li, Y. Su, W. Cui, Y. Huang, M. Cai, B. Zhu, Forensic efficiency evaluation of a mtDNA whole genome sequencing system constructed with long fragment amplification strategy on DNA nanoball sequencing platform, Forensic Sci. Int. Genet. 73 (2024) 103126, https://doi.org/10.1016/j.fsigen.2024.103126.
[15] J. Krause, Q. Fu, J.M. Good, B. Viola, M.V. Shunkov, A.P. Derevianko, S. Pääbo, The complete mitochondrial DNA genome of an unknown hominin from southern Siberia, Nature 464 (2010) 894–897, https://doi.org/10.1038/nature08976.
[16] H.A. Burbano, E. Hodges, R.E. Green, A.W. Briggs, J. Krause, M. Meyer, J.M. Good, T. Maricic, P.L. Johnson, Z. Xuan, M. Rooks, A. Bhattacharjee, L. Brizuela, F. W. Albert, M. de la Rasilla, J. Fortea, A. Rosas, M. Lachmann, G.J. Hannon, S. Pääbo, Targeted investigation of the Neandertal genome by array-based sequence capture, Science 328 (2010) 723–725, https://doi.org/10.1126/science.1188046.
[17] A.W. Briggs, J.M. Good, R.E. Green, J. Krause, T. Maricic, U. Stenzel, S. Pääbo, Primer extension capture: targeted sequence retrieval from heavily degraded DNA sources, J. Vis. Exp. (31) (2009) 1573, https://doi.org/10.3791/1573.
[18] M. Eduardoff, C. Xavier, C. Strobl, A. Casas-Vargas, W. Parson, Optimized mtDNA Control region primer extension capture analysis for forensically relevant samples and highly compromised mtDNA of different age and origin, Genes (Basel) 8 (2017) 237, https://doi.org/10.3390/genes8100237.
[19] C. Strobl, M. Eduardoff, M.M. Bus, M. Allen, W. Parson, Evaluation of the precision ID whole MtDNA genome panel for forensic analyses, Forensic Sci. Int. Genet. 35 (2018) 21–25, https://doi.org/10.1016/j.fsigen.2018.03.013.
[20] A.E. Woerner, A. Ambers, F.R. Wendt, J.L. King, R.S. Moura-Neto, R. Silva, B. Budowle, Evaluation of the precision ID mtDNA whole genome panel on two massively parallel sequencing systems, Forensic Sci. Int. Genet. 36 (2018) 213–224, https://doi.org/10.1016/j.fsigen.2018.07.015.
[21] V. Pereira, A. Longobardi, C. Børsting, Sequencing of mitochondrial genomes using the Precision ID mtDNA Whole Genome Panel, Electrophoresis 39 (2018) 2766–2775, https://doi.org/10.1002/elps.201800088.
[22] E. Avila, P. Graebin, G. Chemale, J. Freitas, A. Kahmann, C.S. Alho, Full mtDNA genome sequencing of Brazilian admixed populations: A forensic-focused evaluation of a MPS application as an alternative to Sanger sequencing methods, Forensic Sci. Int. Genet. 42 (2019) 154–164, https://doi.org/10.1016/j.fsigen.2019.07.004.
[23] M.M. Buś, M. Lembring, A. Kjellström, C. Strobl, B. Zimmermann, W. Parson, M. Allen, Mitochondrial DNA analysis of a Viking age mass grave in Sweden, Forensic Sci. Int. Genet. 42 (2019) 268–274, https://doi.org/10.1016/j.fsigen.2019.06.002.
[24] C. Strobl, J. Churchill Cihlar, R. Lagacé, S. Wootton, C. Roth, N. Huber, L. Schnaller, B. Zimmermann, G. Huber, S. Lay Hong, R. Moura-Neto, R. Silva, F. Alshamali, L. Souto, K. Anslinger, B. Egyed, R. Jankova-Ajanovska, A. Casas-Vargas, W. Usaquén, D. Silva, C. Barletta-Carrillo, D.H. Tineo, C. Vullo, R. Würzner, C. Xavier, L. Gusmão, H. Niederstätter, M. Bodner, B. Budowle, W. Parson, Evaluation of mitogenome sequence concordance, heteroplasmy detection, and haplogrouping in a worldwide lineage study using the Precision ID mtDNA Whole Genome Panel, Forensic Sci. Int. Genet. 42 (2019) 244–251, https://doi.org/10.1016/j.fsigen.2019.07.013.
[25] M. Wang, Z. Wang, G. He, S. Wang, X. Zou, J. Liu, F. Wang, Z. Ye, Y. Hou, Whole mitochondrial genome analysis of highland Tibetan ethnicity using massively parallel sequencing, Forensic Sci. Int. Genet. 44 (2020) 102197, https://doi.org/10.1016/j.fsigen.2019.102197.
[26] D. Cuenca, J. Battaglia, M. Halsing, S. Sheehan, Mitochondrial sequencing of missing persons DNA casework by implementing thermo fisher's precision ID mtDNA Whole Genome Assay, Genes (Basel) 11 (2020) 1303, https://doi.org/10.3390/genes11111303.
[27] J.C. Cihlar, C. Amory, R. Lagacé, C. Roth, W. Parson, B. Budowle, Developmental Validation of a MPS Workflow with a PCR-Based Short Amplicon Whole Mitochondrial Genome Panel, Genes (Basel) 11 (2020) 1345, https://doi.org/10.3390/genes11111345.
[28] J.C. Cihlar, C. Strobl, R. Lagacé, M. Muenzler, W. Parson, B. Budowle, Distinguishing mitochondrial DNA and NUMT sequences amplified with the precision ID mtDNA whole genome panel, Mitochondrion 55 (2020) 122–133, https://doi.org/10.1016/j.mito.2020.09.001.

[29] C. Faccinetto, D. Sabbatini, P. Serventi, M. Rigato, C. Salvoro, G. Casamassima, G. Margiotta, S. De Fanti, S. Sarno, N. Staiti, D. Luiselli, A. Marino, G. Vazza, Internal validation and improvement of mitochondrial genome sequencing using the Precision ID mtDNA Whole Genome Panel, Int. J. Leg. Med. 135 (2021) 2295–2306, https://doi.org/10.1007/s00414-021-02686-w.
[30] A. Ambers, K. Elwick, E.R. Cropper, M.D. Brandhagen, B. Jones, J. Durst, K. K. Gilmore, J.E. Bruseth, H. Gill-King, Mitochondrial DNA analysis of the putative skeletal remains of Sieur de Marle: Genetic support for anthropological assessment of biogeographic ancestry, Forensic Sci. Int. 320 (2021) 110682, https://doi.org/10.1016/j.forsciint.2021.110682.
[31] C.L. Holt, K.M. Stephens, P. Walichiewicz, K.D. Fleming, E. Forouzmand, S.F. Wu, Human mitochondrial control region and mtgenome: design and forensic validation of NGS multiplexes, sequencing and analytical software, Genes (Basel) 12 (2021) 599, https://doi.org/10.3390/genes12040599.
[32] D. Peng, J. Geng, J. Yang, J. Liu, N. Wang, R. Wu, H. Sun, Whole mitochondrial genome detection and analysis of two- to four-generation maternal pedigrees using a new massively parallel sequencing panel, Genes (Basel) 14 (2023) 912, https://doi.org/10.3390/genes14040912.
[33] G. Liu, Y. Zheng, Q. Wu, T. Feng, Y. Xia, D. Chen, L. Ren, X. Bai, Q. Li, D. Chen, M. Lv, M. Liao, W. Liang, L. Zhang, S. Qu, Assessment of ForenSeq mtDNA Whole Genome Kit for forensic application, Int. J. Leg. Med. 137 (2023) 1693–1703, https://doi.org/10.1007/s00414-023-03084-0.
[34] R.R. Zascavage, C.L. Hall, K. Thorson, M. Mahmoud, F.J. Sedlazeck, J.V. Planz, Approaches to whole mitochondrial genome sequencing on the oxford nanopore MinION, Curr. Protoc. Hum. Genet. 104 (2019) e94, https://doi.org/10.1002/cphg.94.
[35] B.R. Karin, S. Arellano, L. Wang, K. Walzer, A. Pomerantz, J.M. Vasquez, K. Chatla, P.H. Sudmant, B.H. Bach, L.L. Smith, J.A. McGuire, Highly-multiplexed and efficient long-amplicon PacBio and Nanopore sequencing of hundreds of full mitochondrial genomes, BMC Genom. 24 (2023) 229, https://doi.org/10.1186/s12864-023-09277-6.
[36] Scientific Working Group on DNA Analysis Methods (SWGDAM), Validation guidelines for DNA analysis methods, SWGDAM, Washington, 2016. Available at: (⟨https://www.swgdam.org/_files/ugd/4344b0_813b241e8944497e99b9c45b163b76bd.pdf⟩).
[37] Thermo Fisher Scientific, AutoMate Express ™ Instrument User Guide, P/N 4441982. Rev.G, Thermo Fisher Scientific, Waltham, 2018. ⟨https://assets.thermofisher.cn/TFS-Assets/LSG/manuals/4441982_AutoMateExp_UG.pdf⟩ (Available at).
[38] Thermo Fisher Scientific, Quantifiler ™ HP and Trio DNA Quantification Kits User Guide, P/N 4485354. Rev.H, , Thermo Fisher Scientific, Waltham, 2018. ⟨https://assets.thermofisher.cn/TFS-Assets/LSG/manuals/4485354.pdf⟩ (Available at).
[39] Verogen, ForenSeq mtDNA Whole Genome Kit Reference Guide, Document # VD2020006 Rev. B, Verogen, San Diego, 2020. ⟨https://verogen.com/wp-content/uploads/2022/06/forenseq-mtdna-whole-genome-kit-reference-guide-vd2020006-b.pdf⟩ (Available at).
[40] Thermo Fisher Scientific, Qubit ® dsDNA HS Assay Kits, P/N MAN0002326. Rev. C.0, Thermo Fisher Scientific, Waltham, 2015. ⟨https://assets.thermofisher.cn/TFS-Assets/LSG/manuals/Qubit_dsDNA_HS_Assay_UG.pdf⟩ (Available at).
[41] Verogen, MiSeq FGx Sequencing System Reference Guide. Document # VD2018006 Rev. F, Verogen, San Diego, 2021. ⟨https://verogen.com/wp-content/uploads/2021/02/miseq-fgx-system-reference-guide-vd2018006-f.pdf⟩ (Available at).
[42] Verogen, Universal Analysis Software v2.0 Reference Guide. Document # VD2019002 Rev. E, Verogen, San Diego, 2021. ⟨https://verogen.com/wp-content/uploads/2021/05/universal-analysis-software-v2-0-reference-guide-vd2019002-e.pdf⟩ (Available at).
[43] J.T. Robinson, H. Thorvaldsdóttir, W. Winckler, M. Guttman, E.S. Lander, G. Getz, J.P. Mesirov, Integrative genomics viewer, Nat. Biotechnol. 29 (2011) 24–26, https://doi.org/10.1038/nbt.1754.
[44] S. Schönherr, H. Weissensteiner, F. Kronenberg, L. Forer, Haplogrep 3 - an interactive haplogroup classification and analysis platform, Nucleic Acids Res. 51 (2023) W263–W268, https://doi.org/10.1093/nar/gkad284.
[45] A. Dür, N. Huber, W. Parson, Fine-Tuning Phylogenetic Alignment and Haplogrouping of mtDNA Sequences, Int. J. Mol. Sci. 22 (2021) 5747, https://doi.org/10.3390/ijms22115747.
[46] M. van Oven, M. Kayser, Updated comprehensive phylogenetic tree of global human mitochondrial DNA variation, Hum. Mutat. 30 (2009) e386–e394, https://doi.org/10.1002/humu.20921.
[47] W. Parson, A. Dür, EMPOP–a forensic mtDNA database, Forensic Sci. Int. Genet. 1 (2007) 88–92, https://doi.org/10.1016/j.fsigen.2007.01.018.
[48] R. Core Team, R: A language and environment for statistical computing, R Foundation for Statistical Computing, Vienna, 2015. Available at: (⟨https://www.r-project.org⟩).
[49] C. Chen, Y. Wu, J. Li, X. Wang, Z. Zeng, J. Xu, Y. Liu, J. Feng, H. Chen, Y. He, R. Xia, TBtools-II: A "one for all, all for one" bioinformatics platform for biological big-data mining, Mol. Plant. 16 (2023) 1733–1742, https://doi.org/10.1016/j.molp.2023.09.010.
[50] J.C. Cihlar, D. Peters, C. Strobl, W. Parson, B. Budowle, The lot-to-lot variability in the mitochondrial genome of controls, Forensic Sci. Int. Genet. 47 (2020) 102298, https://doi.org/10.1016/j.fsigen.2020.102298.
[51] K. Ma, X. Zhao, H. Li, Y. Cao, W. Li, J. Ouyang, L. Xie, W. Liu, Massive parallel sequencing of mitochondrial DNA genomes from mother-child pairs using the ion torrent personal genome machine (PGM), Forensic Sci. Int. Genet. 32 (2018) 88–93, https://doi.org/10.1016/j.fsigen.2017.11.001.
[52] W. Parson, L. Gusmão, D.R. Hares, J.A. Irwin, W.R. Mayr, N. Morling, E. Pokorak, M. Prinz, A. Salas, P.M. Schneider, T.J. Parsons, DNA Commission of the International Society for Forensic Genetics: revised and extended guidelines for mitochondrial DNA typing, Forensic Sci. Int. Genet. 13 (2014) 134–142, https://doi.org/10.1016/j.fsigen.2014.07.010.
[53] A. Dür, N. Huber, W. Parson, Fine-Tuning Phylogenetic Alignment and Haplogrouping of mtDNA Sequences, Int. J. Mol. Sci. 22 (2021) 5747, https://doi.org/10.3390/ijms22115747.
[54] Scientific Working Group on DNA Analysis Methods (SWGDAM), Interpretation Guidelines for Mitochondrial DNA Analysis by Forensic DNA Testing Laboratories, SWGDAM, Washington, 2019. ⟨https://www.swgdam.org/_files/ugd/4344b0_f61de6abf3b94c52b28139bff600ae98.pdf⟩ (Available at).
[55] Scientific Working Group on DNA Analysis Methods (SWGDAM), Mitochondrial DNA Nomenclature Examples Document, SWGDAM, Washington, 2015. ⟨https://www.swgdam.org/_files/ugd/4344b0_2044739c57574dbea97f2f85b6f73c9d.pdf⟩ (Available at).
[56] K. Sturk-Andreaggi, W. Parson, M. Allen, C. Marshall, Impact of the sequencing method on the detection and interpretation of mitochondrial DNA length heteroplasmy, Forensic Sci. Int. Genet. 44 (2020) 102205, https://doi.org/10.1016/j.fsigen.2019.102205.
[57] R.S. Just, J.A. Irwin, W. Parson, Mitochondrial DNA heteroplasmy in the emerging field of massively parallel sequencing, Forensic Sci. Int. Genet. 18 (2015) 131–139, https://doi.org/10.1016/j.fsigen.2015.05.003.
[58] R.S. Just, M.K. Scheible, S.A. Fast, K. Sturk-Andreaggi, A.W. Röck, J.M. Bush, J. L. Higginbotham, M.A. Peck, J.D. Ring, G.E. Huber, C. Xavier, C. Strobl, E.A. Lyons, T.M. Diegoli, M. Bodner, L. Fendt, P. Kralj, S. Nagl, D. Niederwieser, B. Zimmermann, W. Parson, J.A. Irwin, Full mtGenome reference data: development and characterization of 588 forensic-quality haplotypes representing three U.S. populations, Forensic Sci. Int. Genet. 14 (2015) 141–155, https://doi.org/10.1016/j.fsigen.2014.09.021.
[59] A. Ramos, C. Santos, L. Mateiu, M. Gonzalez Mdel, L. Alvarez, L. Azevedo, A. Amorim, M.P. Aluja, Frequency and pattern of heteroplasmy in the complete human mitochondrial genome, PLoS One 8 (2013) e7436, https://doi.org/10.1371/journal.pone.0074636.
[60] M. Li, A. Schönberg, M. Schaefer, R. Schroeder, I. Nasidze, M. Stoneking, Detecting heteroplasmy from high-throughput sequencing of complete human mitochondrial DNA genomes, Am. J. Hum. Genet. 87 (2010) 237–249, https://doi.org/10.1016/j.ajhg.2010.07.014.
[61] M. Li, R. Schröder, S. Ni, B. Madea, M. Stoneking, Extensive tissue-related and allele-related mtDNA heteroplasmy suggests positive selection for somatic mutations, Proc. Natl. Acad. Sci. U. S. A. 112 (2015) 2491–2496, https://doi.org/10.1073/pnas.1419651112.
[62] J.A. Irwin, J.L. Saunier, H. Niederstatter, K.M. Strouss, K.A. Sturk, T.M. Diegoli, A. Brandstätter, W. Parson, T.J. Parsons, Investigation of heteroplasmy in the human mitochondrial DNA control region: a synthesis of observations from more than 5000 global population samples, J. Mol. Evol. 68 (2009) 516–527, https://doi.org/10.1007/s00239-009-9227-4.
[63] S. Riman, K.M. Kiesler, L.A. Borsuk, P.M. Vallone, Characterization of NIST human mitochondrial DNA SRM-2392 and SRM-2392-I standard reference materials by next generation sequencing, Forensic Sci. Int. Genet. 29 (2017) 181–192, https://doi.org/10.1016/j.fsigen.2017.04.005.
[64] M. Obal, T. Zupanc, I. Zupanič Pajnič, Measure quantity of mitochondrial DNA in aged bones or calculate it from nuclear DNA quantitative PCR results? Int. J. Leg. Med. 137 (2023) 1653–1659, https://doi.org/10.1007/s00414-023-03074-2.
[65] F. Guo, Y. Lang, G. Long, Z. Liu, G. Jing, Y. Zhou, B. Zhang, S. Yu, Ion Torrent ™ Genexus ™ Integrated Sequencer and ForeNGS Analysis Software-An automatic NGS-STR workflow from DNA to profile for forensic science, Forensic Sci. Int. Genet. 61 (2022) 102753, https://doi.org/10.1016/j.fsigen.2022.102753.
[66] F. Guo, G. Jing, Y. Lang, Z. Liu, S. Yu, Simultaneous sequencing of 102 Y-STRs on Ion Torrent ™ GeneStudio ™ S5 System, Forensic Sci. Int. Genet. 71 (2024) 103059, https://doi.org/10.1016/j.fsigen.2024.103059.
[67] K.L. Opel, D. Chung, B.R. McCord, A study of PCR inhibition mechanisms using real time PCR, J. Forensic Sci. 55 (2010) 25–33, https://doi.org/10.1111/j.1556-4029.2009.01245.x.
[68] F. Guo, J. Yu, L. Zhang, J. Li, Massively parallel sequencing of forensic STRs and SNPs using the Illumina® ForenSeq™ DNA Signature Prep Kit on the MiSeq FGx™ Forensic Genomics System, Forensic Sci. Int. Genet. 31 (2017) 135–148, https://doi.org/10.1016/j.fsigen.2017.09.003.
[69] M.G. Ensenberger, C.R. Hill, R.S. McLaren, C.J. Sprecher, D.R. Storts, Developmental validation of the PowerPlex(®) 21 System, Forensic Sci. Int. Genet. 9 (2014) 169–178, https://doi.org/10.1016/j.fsigen.2013.12.005.
[70] S. Lee, P.K. McAnany, C.W. Chang, W. Norona, M.L. Short, J.J. Mulero, C. Zhong, Developmental validation of applied biosystems yfiler platinum casework PCR amplification kit, Sci. Rep. 13 (2023) 14539, https://doi.org/10.1038/s41598-023-41788-w.
[71] C. Marshall, W. Parson, Interpreting NUMTs in forensic genetics: Seeing the forest for the trees, Forensic Sci. Int. Genet. 53 (2021) 102497, https://doi.org/10.1016/j.fsigen.2021.102497.
[72] L.C. Canale, J.A. McElhoe, G. Dimick, K.M. DeHeer, J. Beckert, M.M. Holland, Routine mitogenome MPS analysis from 1 and 5 mm of rootless human hair, Genes (Basel) 13 (2022) 2144, https://doi.org/10.3390/genes13112144.
[73] M.D. Brandhagen, O. Loreille, J.A. Irwin, Fragmented nuclear DNA is the predominant genetic material in human hair shafts, Genes (Basel) 9 (2018) 640, https://doi.org/10.3390/genes9120640.
[74] S. Desmyter, M. Bodner, G. Huber, S. Dognaux, C. Berger, F. Noël, W. Parson, Hairy matters: MtDNA quantity and sequence variation along and among human head

hairs, Forensic Sci. Int. Genet. 25 (2016) 1–9, https://doi.org/10.1016/j.fsigen.2016.07.012.